



Bio-based synthesis of silver nanoparticles using leaf extract of *Uraria picta* (Jacq.) Desv. ex DC.: Characterization and evaluation of its activity against *Leishmania donovani*

Jyoti Dixit¹ · Pradeep Kumar¹ · Rajan Singh² · Pooja Verma¹ · Kavindra Nath Tiwari¹ · Rakesh Kumar Singh² · Sunil Kumar Mishra³ · Jasmeet Singh⁴

Received: 24 January 2024 / Revised: 29 April 2024 / Accepted: 5 May 2024
© The Author(s), under exclusive licence to Springer-Verlag GmbH Germany, part of Springer Nature 2024

Abstract

Uraria picta is used as a folk medicine to cure various ailments. Regardless of ethnobotanical application, a therapeutic study of the plant parts has yet to be reported. Aqueous leaf extract was enriched with secondary metabolites like phenols, alkaloids, and terpenoids. Total phenol ($60.97 \text{ mgG}^{-1} \text{ GAE}$), total flavonoid ($52.36 \text{ mgG}^{-1} \text{ RE}$), and antioxidant activity ($\text{IC}_{50} 2666.95 \mu\text{g mL}^{-1}$) of the extract were measured. Bio-based silver nanoparticles (LEUP-AgNPs) were fabricated using a secondary metabolite-enriched leaf extract of *U. picta* (LEUP), and characterization of LEUP-AgNPs was done. The LEUP-AgNPs were crystalline, circular ($13.04 \pm 5.97 \text{ nm}$), monodisperse (pdi 0.205), and stable (-17.8 mV). The LEUP-AgNPs surface was composed of carbon, nitrogen, oxygen, and silver. A comparative study was performed to evaluate the potential of LEUP and LEUP-AgNPs against promastigotes and intra-RAW264.7 macrophage amastigotes of *Leishmania donovani*. A high dose of LEUP and LEUP-AgNPs significantly inhibited the growth of promastigotes up to 53% and 68%, with an IC_{50} value of $47.90 \mu\text{g mL}^{-1}$ and $6.79 \mu\text{g mL}^{-1}$, respectively. LEUP and LEUP-AgNPs higher doses also inhibited intracellular amastigotes up to 53% and 80% with an IC_{50} value of $6.72 \mu\text{g mL}^{-1}$ and $1.16 \mu\text{g mL}^{-1}$, respectively. The microscopic examination revealed that LEUP-AgNPs lead to size reduction and aggregations of promastigotes. The LEUP-AgNPs efficiently declined the number of amastigotes per RAW 264.7 macrophages compared to LEUP. LEUP-AgNPs had no cytotoxic effects on RAW 264.7 macrophages based on the CC_{50} value. Findings showed LEUP-AgNPs were more efficient than LEUP in controlling *L. donovani*, which induces visceral leishmaniasis.

Keywords Anti-leishmanial · Aqueous leaf extract · *Leishmania donovani* · Nanoparticles · Promastigotes · *Uraria picta*

Abbreviations

LEUP	Leaf extract of <i>Uraria picta</i>	HR-TEM	High Resolution-Transmission Electron Microscopy
LEUP-AgNPs	Silver nanoparticles synthesized through leaf extract of <i>U. picta</i>	HR-SEM	High Resolution-Scanning Electron Microscopy
		DLS	Dynamic Light Scattering

✉ Kavindra Nath Tiwari
kntiwari@bhu.ac.in; kntiwaribhu@gmail.com

- ¹ Department of Botany, MMV, Banaras Hindu University, Varanasi 221005, India
- ² Department of Biochemistry, Institute of Science, Banaras Hindu University, Varanasi 221005, India
- ³ Department of Pharmaceutical Engineering and Technology, Indian Institute of Technology-Banaras Hindu University, Varanasi 221005, India
- ⁴ Department of Dravyaguna, Institute of Medical Science, Banaras Hindu University, Varanasi 221005, India

1 Introduction

Uraria picta is a valuable medicinal herb and a key ingredient in many herbal formulations [1]. It is a member of the Fabaceae family. In India, it is referred to as Prishniparni and Pithvan. The plant's leaves are utilized as diuretics, aphrodisiacs, and antiseptics [2]. The leaves were used to treat oral sores [3]. Based on reports of pharmacological studies, the extracts of plant parts have acaricidal [4], antimicrobial [5], bone healing [6], antioxidant, anticholinesterase [7],

free radical scavenging [8], and antianxiety properties [9]. It cures gonorrhoea [10] and gynaecological disorders [3].

Visceral leishmaniasis (VL) is the second-most prevalent zoonosis on earth. *Leishmania donovani* is the protozoan parasite that is responsible for causing VL. VL is the leishmaniasis variant that is the most virulent. It has the potential to spread quickly, leading to an epidemic and increased mortality. The illness is often called Kala-azar, black fever, or deadly fever. During VL, the dermal layer of body parts becomes thick and dark in color. As VL progresses, it impairs the normal operation of various vital organs, including the liver, spleen, small intestinal mucosa, bone marrow, and lymph nodes [11]. VL also causes the development of several health-related complications, such as reticuloendothelial hyperplasia. VL could cause outbreaks and scale up mortality if it is not treated. VL is endemic in seventy-nine countries. Countries like Somalia, Brazil, Ethiopia, South Sudan, Yemen, Eritrea, India, China, and Kenya contributed ninety percent of all new VL cases [12]. Globally, there are $5\text{--}9 \times 10^4$ recorded cases of VL per year. There are about twenty different species of *Leishmania* [13]. VL is spread via the sting of infected female phlebotomine sandflies [14]. Chemotherapy is the chief method used to control leishmaniasis worldwide. The medication for VL involves amphotericin B, miltefosine, meglumine antimoniate, sodium stibogluconate, pentamidine, and paromomycin [15]. Poor efficacy, accumulation of toxic compounds in macrophages, insufficient antigen presentation to immune cells, systemic toxicity, prolonged course, and cost of treatment are the main limitations of conventional therapy [16].

The commencement of nanotechnology in pharmaceuticals has efficiently upgraded diagnostic, preventive, and treatment measures with a significant effect on human health [17]. In the biological environment, therapeutic and diagnostic compounds encapsulated with nano-meter-sized particles improve their sensitivity, specificity, and effectiveness towards their targets [18]. The benefits of nanomedicine include the potential to reach areas like the tumor's micro-environment and easy dissipation without causing toxicity. Several nanomedicines like synthon, nab-paclitaxel, yttrium-90 radiolabeled ibritumomab tiuxetan, copaxone, and glatiramer acetate are commercially used for the management of various critical cancer diseases [19].

Nanotechnology has been used to produce different types of nanomaterials. Nanomaterials should have a maximum size of 100 nm. Nanoparticles are categorized into groups based on their unique forms [20]. These are frequently employed for different purposes, like drug transportation and sensing organic and chemical samples [21]. Due to their specific size and mode of action, nanomaterial applications regularly increase in the field of medicine [22]. The limitations of anti-leishmania formulations can be overcome by developing nanomedicine targeted against the leishmania

parasite. Nanomedicine's application in medical science has emerged as a new hope against antimicrobial resistance [22]. Based on their structure, composition, and physicochemical characteristics, different kinds of nano-drug transport structures have been developed for anti-leishmanial activity. The important nano-drug transport structures include liposomes, transferosomes, niosomes, carbon nanotubes, solid lipid nanoparticles (NPs), polymeric NPs, mesoporous silica NPs, and metallic NPs [23]. To synthesize nanoparticles, many metals like gold, silver, zinc, titanium, and magnesium are employed [24]. Metallic nanoparticles are being formulated based on the antimicrobial properties of both essential and non-essential metals.

Silver nanoparticles (AgNPs) are the preferred choice among metal nanoparticles for their stability, high surface area per unit volume, and broad-spectrum antibacterial activity [25, 26]. These qualities encourage the production of AgNPs. The physical processes are costly, multistep, prolonged, require a lot of space, and dissipate enormous amounts of energy that enhance the environment's temperature. However, chemical methods generate toxic waste in the environment [27]. Bio-based materials are rich in secondary metabolites. The presence of biologically active compounds in bio-based materials enhanced their role against a wide spectrum of diseases, deficiencies, and biological activities [28]. They are good reducing and coating agents for green nanoparticle synthesis [29].

Bio-based synthesized silver nanoparticles have attracted a lot of attention because of their negligible harmful effects, biological compatibility, simple synthesis, high surface area, electrical conductivity, magnetic properties, and ease of isolation. The bio-based method of silver nanoparticle fabrication is cost-effective, requires a short duration, and enhances the therapeutic value [30]. Bio-based green synthesized silver nanoparticles were used in the management of health issues like cancer [31], neurodegenerative disease [32], and malaria [33]. Bio-based materials are enriched with diversified phytoconstituents that are toxic to microbial agents [29]. Silver nanoparticles synthesized through bio-based materials have potential anti-microbial properties against bacterial [34], protozoan [35], and fungal [36] pathogens. Such vital characteristics of these bio-based silver nanoparticles improve their biological activity and provide wide applications for pharmaceutical purposes [37].

Based on the previous studies, bio-based extracts or green synthesized nanoparticles were used to study the effect only on the promastigotes form of *L. donovani*. There are no previous reports on the effect of the clinically important amastigote phase of the parasite *L. donovani*. A few reports of the anti-leishmanial properties of plant-based materials such as extracts of *Embilica officinalis* [38], *Putranjiva roxburghii* [39], and *Corchorus capsularis* [40] were based on the inhibition of the promastigotes form of *L. donovani*. The

IC₅₀ values of the extracts in these reports range from 21.6 µg mL⁻¹ to 79.0 µg mL⁻¹. There are only three reports of the anti-leishmanial property of bio-based synthesized silver nanoparticles against the promastigotes form of *L. donovani*. Green biosynthesized nanoparticles were not tested against the amastigote phase of the parasite *L. donovani* in most of the cases. *Euphorbia prostrata* [41], *Xanthium strumarium* [42], and *Sechium edule* [43] extract-mediated AgNPs showed IC₅₀ values of 14.94 µg mL⁻¹, 8.93 µg mL⁻¹, and 51.88 µg mL⁻¹, respectively, against the promastigotes form of *L. donovani*. In a report, gold nanoparticles were tested against promastigotes, with IC₅₀ values of 40 µM [44]. In a single report, the efficacy of arsenic nanoparticles was evaluated against promastigotes as well as amastigote forms of pathogen with an IC₅₀ value of 23.4 µM and 1.5 µM, respectively [45].

There is no report of anti-leishmanial activity of *U. picta* and its mediated silver nanoparticles against *Leishmania donovani* to date. Lately, the antibacterial activity of silver nanoparticles fabricated from *U. picta* leaf extract has been studied [46]. The objective of the present investigation was to study the qualitative phytochemical analysis and quantitative assessment of the total phenol and total flavonoid content of the aqueous leaf extract of *U. picta*. Bio-based AgNPs were fabricated using leaf extract in the current study. The leaf extract and its fabricated AgNPs were tested against both promastigotes as well as amastigote forms of *Leishmania donovani* to evaluate its efficacy for the management of visceral leishmaniasis. The cytotoxicity assessment of bio-based fabricated AgNPs of *U. picta* is also studied against RAW264.7 mouse macrophages, which is lacking in previous reports.

2 Materials and methods

2.1 Preparation of leaf extract

The *U. picta* leaves were harvested in good health from the Ayurveda field of the Department of Dravyaguna, Banaras Hindu University in Varanasi, India. *U. picta* was authenticated (Accession no. 104329) by the Botanical Survey of India, Allahabad, India. After thoroughly washing, the leaves were dried in shed conditions at 24 ± 2 °C. The leaves were pulverized. Powder (25 g) was mixed with 100 mL deionized purified water (distillation unit, USIC level II, BHU) and placed for 30 min at 40 °C. The leaf extract of *U. picta* (LEUP) was kept at 24 ± 2 °C for a few minutes. The LEUP was sieved by Whatman filter paper No. 1 and maintained at 4 °C for the bio-based fabrication of silver nanoparticles. For the phytochemical analysis, LEUP was concentrated at 40 °C through a rotatory evaporator.

2.2 Phytochemical analysis of LEUP

2.2.1 Qualitative phytochemical analysis

The LEUP (2 mL) was added to 2 mL of ferric chloride solution. The reaction turned green or blue. It showed the occurrence of phenols. The LEUP (2 mL) was added to 2 mL hydrochloric acid. The reaction was boiled and kept at 24 ± 2 °C to cool down. Two drops of Wagner's reagent were poured into the reaction mixture. The reaction was turned to brown-red. It indicated the occurrence of alkaloids. The LEUP (2 mL) was dried at 60 °C. The dry LEUP was dissolved in 1 mL of distilled water and shaken vigorously. The formation of persistent foam indicated the presence of saponin. The LEUP (2 mL) was added to 2 mL of chloroform. A few drops of H₂SO₄ were added to the reaction mixture. The appearance of a red-brown color indicated the presence of terpenoids. The LEUP (5 mL) was added to 2 mL of CHCl₃. The concentrated H₂SO₄ (3 mL) was added to the reaction mixture. It showed the presence of steroids [47]. The LEUP (2 mL) was added to 10% NaOH (3 mL). The reaction turned yellow. It showed the presence of coumarin. The LEUP (2 mL) was added to 40% NaOH (1 mL). A few drops (2–3) of 1% CuSO₄ were added to the reaction mixture. It showed the presence of protein [48].

2.2.2 Estimation of total phenol and flavonoid in LEUP

Different concentrations (100–1000 µg mL⁻¹) of LEUP were prepared. Reactions through each LEUP concentration were conducted. LEUP (100 µL) was added to 1 mL distilled water. Folin ciocalteu solution (200 µL) was added. The reaction mixture was mixed and kept for 8 min. Sodium carbonate (7%, 2 mL) and double distilled water (700 µL) was added. The reaction was kept for 15 min. The absorbance of the reaction was noted at 750 nm. The total phenol content (TPC) in LEUP was determined through the standard curve of Gallic acid. TPC was expressed as a milligram per gram of Gallic acid equivalent (GAE) [49].

LEUP (100 µL) was added to AlCl₃ (2%, 100 µL). Potassium acetate (1 M, 100 µL) and ethyl alcohol (2.7 mL) was added. The reaction was kept at 37 °C for 30 min. The absorbance of the reaction was noticed at 415 nm. The total flavonoid content (TFC) was determined through the standard curve of Rutin. TFC was expressed as milligram per gram of Rutin equivalent (RE) [49].

2.3 Bio-based synthesis of LEUP-AgNPs

For the bio-based fabrication of LEUP-AgNPs, 1 mL of LEUP was supplemented with 100 mL of AgNO₃ (1 mM). The reaction was placed under sunlight (65,000 Lux; 38 °C). The reaction mixture became yellowish to golden-brownish,

which indicated LEUP-AgNPs were being synthesized. To track the fabrication of LEUP-AgNPs, a UV–visible spectrophotometer (Shimadzu UV 1800, made in Japan) was utilized to obtain the spectrum of LEUP-AgNPs between 250 and 700 nm. Estimates of the band gap of LEUP-AgNPs were made via the Tauc plot. The following Tauc relation was used to plot:

$$\alpha h\nu = A(h\nu - E_g)^n$$

Where α = absorption coefficient, h = Planck's constant, ν = frequency of light, A = absorbance, E_g = optical band gap, and $n = 2$ or $1/2$ (index value based on direct and indirect allowed transition).

The factors such as photoperiod (5–30 min), LEUP inoculum concentration (0.25–4%), silver salt concentration (0.5–5 mM), and pH (4–10) of the reaction were optimized for optimal biosynthesis of silver nanoparticles because they affect the synthesis, yield, and quality (shape and size) of bio-based synthesized LEUP-AgNPs. The LEUP-AgNPs reaction mixture was centrifuged at 11,200 g for 10 min to extract LEUP-AgNPs. The pellet obtained was thoroughly washed with Millipore water to eliminate the impurities. The pellet was dehydrated at 60 °C and utilized for LEUP-AgNPs analysis.

2.4 Analytical strategies to define LEUP-AgNPs

Fourier transform infrared spectroscopy (FTIR; developed in Germany by Burker) was used to identify different clusters of atoms and bonds present in the LEUP and LEUP-AgNPs. The recognition of LEUP functional groups involved in interaction with silver nitrate to reduce Ag^+ to Ag^0 was achieved through the FTIR study. The LEUP and LEUP-AgNPs infrared spectra were determined to be in the 4000–400 cm^{-1} region. The LEUP-AgNP crystallographic behaviour was examined through an X-ray diffractometer (XRD; Rigaku Miniflex 600). The crystalline size of LEUP-AgNPs was calculated through the Debye–Scherrer equation:

$$D = (K\lambda)/\beta\cos\theta,$$

Where D is the mean crystallite size; K is Scherrer's constant; λ is wavelength of X-ray; β is full width at the half maximum of the diffraction peak; θ is diffraction angle. The microstructures and crystalline properties of LEUP-AgNPs were observed via high-resolution transmission electron microscopy (HR-TEM; FEI, TECNAI 20, G2) associated with selected area electron diffraction (SAED). The HR-TEM was run at a 120 kV accelerated voltage. The LEUP-AgNPs preparation for HR-TEM was done by coating a thin layer of LEUP-AgNPs over a copper grid and placing it to dry at 24 ± 2 °C for 30 min. Morphological characters (shape

and size) of LEUP-AgNPs were examined through scanning electron microscopy (SEM; ZEISS-EVO MA 15, Japan) and recorded at 10 kV with a consistent supply of 1 nA for 7 s. Energy dispersive X-ray (EDX) verified the purity of the chemical makeup of LEUP-AgNPs by spectral analysis. The topological investigation of LEUP-AgNPs was carried out by atomic force microscopy (AFM; NT-MDT, Russia). A sample for surface properties examination was prepared by pouring LEUP-AgNPs solution (a drop) on a glass slide (approx. $1 \times 1 \text{ cm}^2$) and keeping it to dry at 24 ± 2 °C. Particle size and polydispersity index of bio-based synthesized LEUP-AgNPs were studied through dynamic light scattering (DLS; NanoPlus Common, Particulate System) at 25 °C with 52,183 cps scattering intensity. The diluent used was water ($n = 1.3328$). The Malvern Zetasizer Nano ZS was utilized for the assessment of the zeta potential of LEUP-AgNPs at 24.9 °C. The surface elemental composition of LEUP-AgNPs was examined through X-ray photoelectron spectroscopy (Thermo Fisher Scientific Inc., USA) using the K Alpha model.

2.5 Antioxidant analysis of LEUP and LEUP-AgNPs

DPPH (0.002%, 3 mL) was added to 100–1000 $\mu\text{g mL}^{-1}$ of LEUP and LEUP-AgNPs separately. The reaction was kept at 24 ± 2 °C for 15 min. Ascorbic acid (100–1000 $\mu\text{g mL}^{-1}$) was used as a standard. The absorbance of the reaction was recorded at 517 nm through a UV–Vis spectrophotometer (SHIMADZU UV 1800ENG240V, SOF) [47].

2.6 Cultures of promastigotes and intra-RAW264.7 macrophages

Promastigote, an infective form of *L. donovani*, was cultivated on Dulbecco's modified eagle's medium (DMEM). Fetal bovine serum (FBS) 10%, penicillin 100 Units mL^{-1} , streptomycin 100 $\mu\text{g mL}^{-1}$, and gentamycin 20 $\mu\text{g mL}^{-1}$ were added to DMEM. The promastigotes culture was incubated at 26 °C. Amastigotes were internalized and nurtured in RAW264.7 macrophages. The intracellular amastigotes were maintained on DMEM augmented with FBS and antibiotics under standard in vitro conditions.

2.6.1 Estimation of anti-promastigotes activity

The stock of LEUP (1 mg mL^{-1}) and LEUP-AgNPs (1 mg mL^{-1}) was prepared in dimethyl sulfoxide (DMSO) individually. The working solutions of LEUP (200 $\mu\text{g mL}^{-1}$) and LEUP-AgNPs (200 $\mu\text{g mL}^{-1}$) were prepared in an incomplete culture medium through respective stock solutions. The different concentrations of LEUP (200–1.5 $\mu\text{g mL}^{-1}$) and LEUP-AgNPs (200–1.5 $\mu\text{g mL}^{-1}$) were maintained through serial dilution. Promastigotes were seeded in a 96-well

microplate at the logarithmic stage (1×10^6 cells, 100 μL per well). Different concentrations (200–1.5 $\mu\text{g mL}^{-1}$) of LEUP and LEUP-AgNPs were added to each well separately. Miltefosine, a phospholipid medication, was offered as a positive control. Following a 24-h incubation period, 0.03 mL of MTT (4 mg mL^{-1}) was poured into each well. It was kept for 4 h at 26 $^\circ\text{C}$. The 96-well plate was spun at 1141 g for 5 min. The upper layer was cast off. Two phases, like supernatant and pellet, were formed, out of which the supernatant was neglected. The pellet was dissolved in 100 μL of DMSO. The per cent inhibition of promastigotes growth was analysed using an ELISA plate reader (Thermo Fisher Scientific, US) at 540 nm. Inhibitory concentrations (IC_{50}) of LEUP and LEUP-AgNPs were determined through regression analysis using GraphPad Prism 9.

2.6.2 Estimation of anti-amastigotes activity

RAW264.7 macrophages (5×10^6 cells, 100 μL per well) were seeded in a 24-well plate and permitted to attach for 5 h. The cells were washed carefully with incomplete DMEM to get rid of non-adherent cells. Promastigotes infected macrophages in a 10:1 ratio. Within 6 h of incubation, the promastigotes had infiltrated the macrophages. Promastigotes outside of macrophages were eliminated by washing with PBS. DMEM was added to the infected macrophages as a supplement. The cultures spent 24 h in a CO_2 incubator. Different concentrations of LEUP (200–1.5 $\mu\text{g mL}^{-1}$) and LEUP-AgNPs (200–1.5 $\mu\text{g mL}^{-1}$) were transferred individually and placed for 24 h in a CO_2 incubator. The anti-amastigote property was determined by the number of intracellular amastigotes per macrophage after Giemsa staining. The IC_{50} was calculated through regression analysis using GraphPad Prism 9.

2.6.3 Estimation of cytotoxicity of LEUP and LEUP-AgNPs

The cytotoxicity of LEUP and LEUP-AgNPs against intra-RAW264.7 macrophage cells was determined. A 96-well microplate was seeded with 1×10^6 cells per well to achieve the half-maximum cytotoxic concentration (CC_{50}). Different concentrations of LEUP (200–1.5 $\mu\text{g mL}^{-1}$) and LEUP-AgNPs (200–1.5 $\mu\text{g mL}^{-1}$) were added in wells individually and then placed at 37 $^\circ\text{C}$ in a CO_2 incubator for 24 h. The cytotoxic concentration (CC_{50}) of LEUP and LEUP-AgNPs that inhibited 50% of macrophage proliferation was evaluated. The selective index (SI) of LEUP and LEUP-AgNPs was calculated for the intra-macrophage amastigotes form. The SI was the fraction between the CC_{50} of a sample against RAW264.7 macrophages and the IC_{50} against the intracellular amastigotes form of *L. donovani*.

2.7 Statistical analysis

To ensure accuracy, every experiment was carried out three times. Results were shown as mean \pm S.E. A regression analysis was performed to calculate the percentage inhibition growth of *L. donovani* through GraphPad Prism 9.

3 Results and discussion

3.1 Qualitative, quantitative phytochemicals analysis and antioxidant activity of LEUP

A variety of bioactive compounds were identified through the qualitative analysis of LEUP. The LEUP was enriched with phenols, alkaloids, coumarin, terpenoids, steroids, and protein. The total phenol content in LEUP was 60.97 mg G^{-1} GAE ($p \leq 0.05$). The total flavonoid content in LEUP was 52.36 mg G^{-1} RE ($p \leq 0.05$) (Fig. 1). The highest concentration of LEUP (1000 $\mu\text{g mL}^{-1}$) showed 21.16% inhibition of DPPH free radicals ($p \leq 0.05$). A similar result was reported with *Stachys parviflora* extract for free radical scavenging potential [50]. The LEUP also scavenged DPPH free radicals (Fig. 2) with an IC_{50} of 2666.95 $\mu\text{g mL}^{-1}$ in comparison with a standard ascorbic acid IC_{50} of 457.91 $\mu\text{g mL}^{-1}$.

3.2 Biosynthesis of LEUP-AgNPs

The confirmation of Ag^+ ion reduction in the LEUP-AgNPs biosynthesis reaction was performed through a UV–Vis spectrophotometer in comparison with the control (LEUP

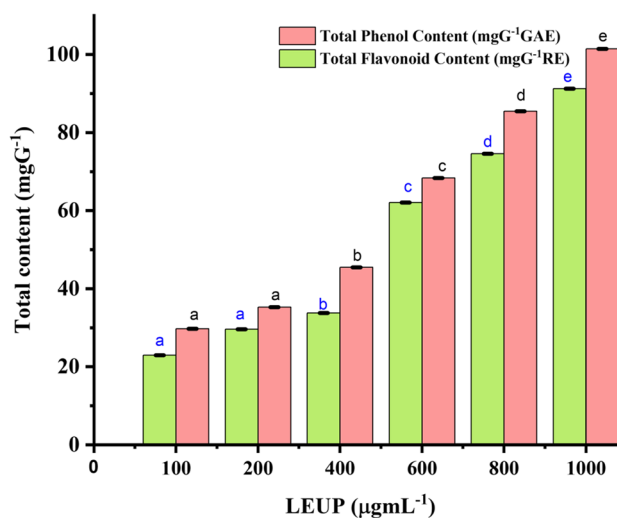


Fig. 1 Total flavonoid and phenol content in LEUP. Data is expressed as mean \pm S.E. The statistical significance difference in data analysed by one way analysis of variance (ANOVA) followed by post hoc Tukey's b test. The alphabetical letters a-e indicates significant difference between the concentrations (at $p < 0.05$)

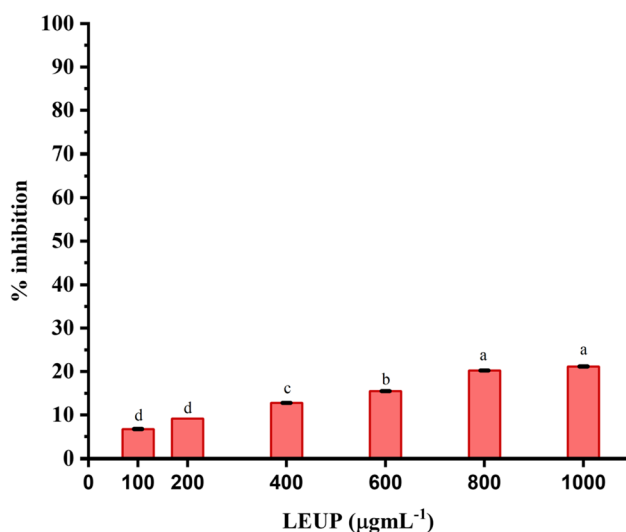


Fig. 2 DPPH free radical per cent inhibition activity of LEUP. Data is expressed as mean \pm S.E. The statistical significance difference in data analysed by one way analysis of variance (ANOVA) followed by post hoc Tukey's b test. The alphabetical letters a-d indicates significant difference between the concentrations (at $p < 0.05$)

and AgNO_3 solution). The LEUP spectrum exhibited two peaks at 280 nm and 320 nm (Fig. 3a). The peaks correspond to the presence of phenolic compounds [51]. It's possible that these secondary metabolites of LEUP donated electrons to silver ions to synthesize colloidal LEUP-AgNPs [52]. The AgNO_3 solution did not show an absorption peak in the same circumstances (Fig. 3a). The change in the colour of the reaction (yellow to brown) indicates the biosynthesis of LEUP-AgNPs when exposed to sunlight (Fig. 3b). The same reaction performed in dark conditions did not show any change in the colour of the reaction mixture. This suggests that sunlight plays a significant role in the biosynthesis of LEUP-AgNPs. The conduction electron of Ag^0 absorbs photons; it gets excited and produces a collective oscillation. This oscillation is called surface plasmon resonance (SPR) [53]. The SPR causes a change in the color of the reaction and indicates a change in silver nitrate's optical properties because the bio-based materials reduce Ag^+ into Ag^0 . The basic methodology used for bio-based fabricated AgNPs is given in Fig. S1. Based on the literature surveyed, AgNP synthesis occurred at 420–470 nm absorption spectra. It was noted that adding LEUP to a 1 mM AgNO_3 solution caused the reaction to turn golden brown (Fig. 3b) under sunlight. A 300–700 nm wavelength range was used to study the LEUP-AgNPs synthesis (Fig. 3a). The construction of a broad SPR apex at 426 nm validated the synthesis of LEUP-AgNPs. Mishra and Kumavat also found the formation of an absorption peak at 425 nm [46].

Tauc plot or graph is a graphical representation used to determine the optical band gap of AgNPs from its

absorption curve. Tauc plot between $h\nu$ and $(\alpha h\nu)^2$ (Fig. 3c) was achieved through absorption curve (Fig. 3b) of LEUP-AgNPs. The band gap of LEUP-AgNPs was determined by drawing a straight line in the chart's linear region where $(\alpha h\nu)^2 = 0$. The band gap of biosynthesized LEUP-AgNPs was 2.10 eV (Fig. 3c). If a silver nanoparticle's band gap value falls between 1.3 and 2.4 eV, it is considered a semiconductor [54]. The band gap property of silver nanoparticles influences their optical and electrical characteristics.

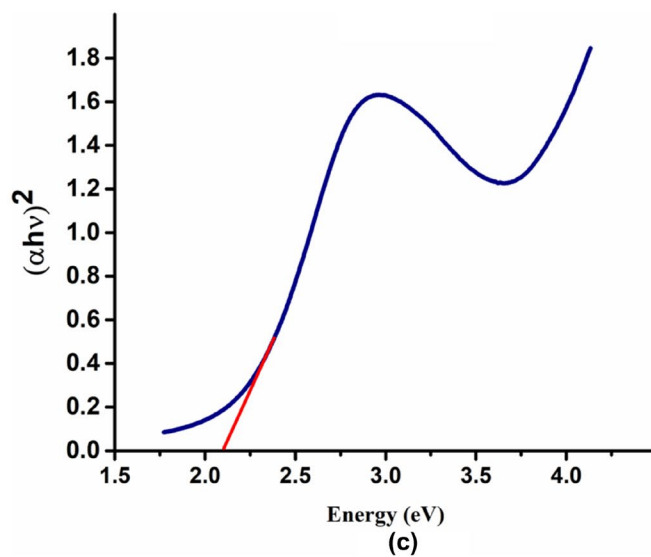
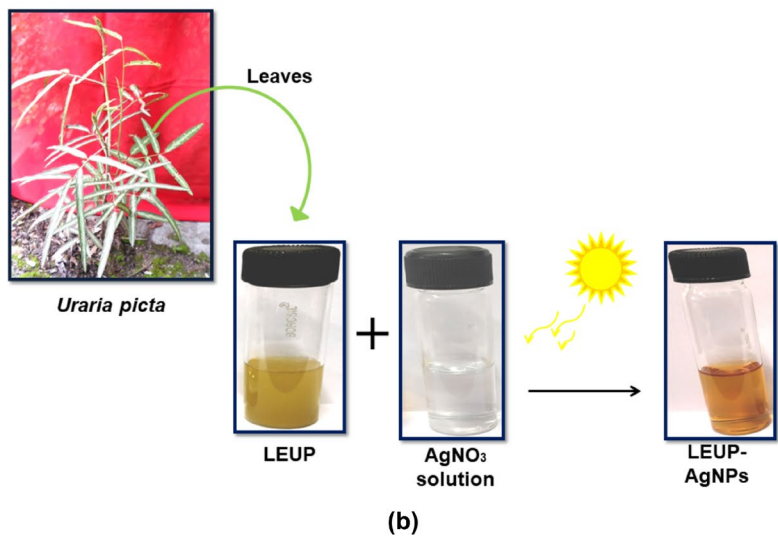
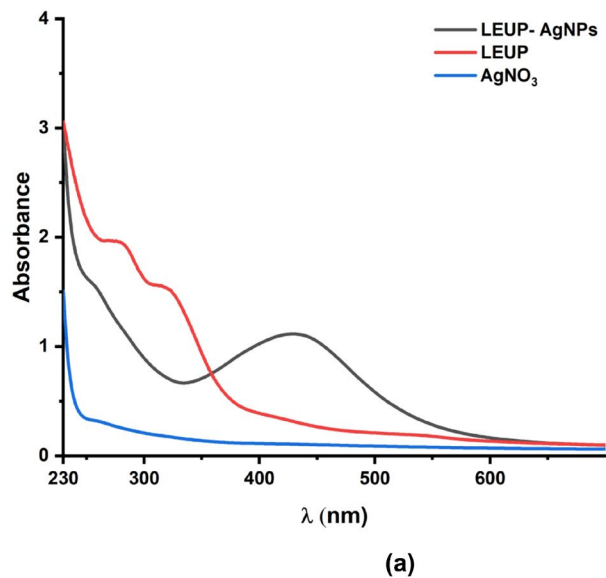
3.2.1 Impact of photoperiod duration on LEUP-AgNPs biosynthesis

The photo-induced LEUP-AgNP fabrication was examined by a UV–Vis absorption spectrophotometer at 5-min intervals. The development of a sharp absorbance apex at 426 nm confirmed the synthesis of LEUP-AgNPs (Fig. S2). The LEUP-AgNPs intensified from yellow to dark reddish brown as the duration of time spent in the sun rose. The SPR peak reallocated from red towards the blue shift region. The absorbance of the SPR peak was high. After 30 min of sun exposure, a prominent SPR band around 426 nm was formed. The SPR of bio-synthesized LEUP-AgNPs depended on the duration of sunlight exposure [55]. As the exposure time to the sunlight increases, the LEUP-AgNP's reaction color darkens from yellow to reddish brown. It was noticed that the 30 min of photoperiod duration were optimal for LEUP-AgNP synthesis.

3.2.2 Impact of LEUP concentration on LEUP-AgNPs biosynthesis

As different LEUP concentrations were added to the AgNO_3 solution, the LEUP-AgNPs interaction took on color. The SPR associated with synthesized LEUP-AgNPs imparts a light yellow, yellow, brown, and reddish-brown color to the reaction mixture [53]. To obtain good-quality LEUP-AgNPs, the effects of various concentrations of LEUP (0.25, 0.5, 1, 2, 3, and 4%) were studied in the reaction mixture containing AgNO_3 (1 mM) solution. The SPR indicates the synthesis of LEUP-AgNPs through different concentrations of LEUP under sunlight for 30 min (Fig. S3). The color of the reaction mixture containing 4% LEUP turned reddish brown. The UV–Vis absorption spectra showed that 4% LEUP in a 1 mM AgNO_3 solution provided the highest SPR peak at 426 nm. A concentration-dependent relationship between LEUP concentration and LEUP-AgNP biosynthesis was noticed. The findings support the concept that plant biomass is potential capping and reducing agent for nanoparticles biosynthesis [56]. Several studies on plant-based AgNP synthesis have been reported, such as *Euphorbia prostrata* [41], *Sargentodoxa cuneata* [57], *Dioscorea bulbifera* [58], and *Maytenus royleanus* [59]. The plant biomass enhanced the

Fig. 3 LEUP-AgNPs bio-based synthesis through *U. picta* leaf extract. **(a)** UV-Visible absorption spectra showing surface plasmon resonance peak of AgNO₃, LEUP, and LEUP-AgNPs. **(b)** Color conversion during reaction. **(c)** Band gap of LEUP-AgNPs



biosynthesized AgNPs' stability, functionality, biocompatibility, communication with biological systems, and biological properties [56].

3.2.3 Impact of AgNO₃ concentration on LEUP-AgNPs biosynthesis

The impact of different AgNO₃ concentrations on LEUP-AgNP fabrication was studied. The molar concentration of Ag⁺ affected the color and absorbance spectra of the LEUP-AgNPs (Fig. S4). The development of darker shades of reddish-brown color was monitored at different AgNO₃ concentrations (0.5–5 mM) for 30 min. For each concentration, a distinct SPR peak of LEUP-AgNPs was obtained (Fig. S4). The SPR peaks (Fig. S4) reflected that with increasing AgNO₃ concentrations, the growth rate of LEUP-AgNPs also increased. At 1 mM AgNO₃ concentration, a prominent SPR peak was observed with the optimum absorbance at 430 nm. With the increase in AgNO₃ concentration (2, 3, and 4 mM), higher SPR peaks were obtained with redshift at λ_{max} (432, 433, and 434 nm, respectively), which might be the result of large LEUP-AgNPs aggregates [55]. At the maximum (5 mM) AgNO₃ concentration, the SPR peak of the AgNPs synthesized was reduced; this could be due to the saturation of reactant (aqueous extract) Ag⁺ ion binding sites [60]. At the minimum (0.5 mM) AgNO₃ concentration, a single and broad SPR peak with the lowest absorbance was monitored [61]. The findings revealed that 1 mM AgNO₃ is the expected optimum concentration for LEUP-AgNPs synthesis.

3.2.4 Impact of pH on LEUP-AgNPs biosynthesis

The fabrication rate of LEUP-AgNPs was influenced by the change in the reaction's pH, as shown in Fig. S5. When 4% LEUP was added to a 1 mM AgNO₃ solution of different pH, the reaction between the extract components and Ag⁺ ions was monitored visually and through a UV–Vis spectrophotometer. The hues of brown and the LEUP-AgNPs' absorbance were both impacted by the AgNO₃ solution's pH change. Such an alteration produced a difference in the rate of LEUP-AgNPs synthesis. The color of the LEUP-AgNPs reaction gradually enhanced from acidic AgNO₃ to alkaline AgNO₃.

At pH 4, 5, and 6 of AgNO₃, the fabrication of LEUP-AgNPs was found to be sluggish. The appearance of a light brown color after 40 to 60 min was visible. At pH 7, the reaction between AgNO₃ and phytocomponents of LEUP initiated immediately. The reaction's light yellow color turned reddish brown. Optimum and stable LEUP-AgNPs were synthesized at 426 nm absorption maxima. The LEUP-AgNPs reaction's hue quickly changed to reddish brown for pH values of 8, 9, and 10 of AgNO₃, with heightened

maxima of absorption occurring at 429, 415, and 431 nm, respectively. The LEUP-AgNPs synthesized were unstable, as they formed aggregates within an hour [61]. The fabrication of substantial LEUP-AgNPs aggregates was signaled by the deep color development and widening of the SPR band. It was noticed that pH 7 of AgNO₃ was optimal for LEUP-AgNPs synthesis.

3.3 Characterization of bio-based synthesized LEUP-AgNPs

3.3.1 FTIR of LEUP-AgNPs

The interaction of functional groups of metabolites existing in the LEUP with silver ions was examined through FTIR analysis. The group frequencies of LEUP and bio-based synthesized LEUP-AgNPs were compared using their respective infrared spectra (Fig. 4). The IR spectrum of LEUP exhibited group frequencies ranging from 3425 to 3631 cm⁻¹ assigned for the O–H stretch of phenols. The bands 2850 and 2926 cm⁻¹ belonged to the methylene C–H asymmetric or symmetric stretch of saturated aliphatic group frequencies. Nitrile C≡N stretch made up the bands 2345 and 2363 cm⁻¹. The bands between 1962 and 1890 cm⁻¹ represented the transition metal carbonyl. The bands between 1867 and 1829 cm⁻¹ belonged to a 5-member ring anhydride. The bands between 1811 and 1776 cm⁻¹ belonged to aryl carbonate. The bands 1750 cm⁻¹ denoted the ester group. Carboxylic acid was ascribed to the bands 1719 and 1703 cm⁻¹. The primary amine N–H bend was located at 1650 cm⁻¹, 1640 cm⁻¹, and 1617 cm⁻¹ [62]. A secondary amine, N–H bend, was found at 1577 cm⁻¹. The bands between 1400 cm⁻¹ and 1362 cm⁻¹ belonged to the phenol or tertiary alcohol O–H bend. The skeletal C–C vibration

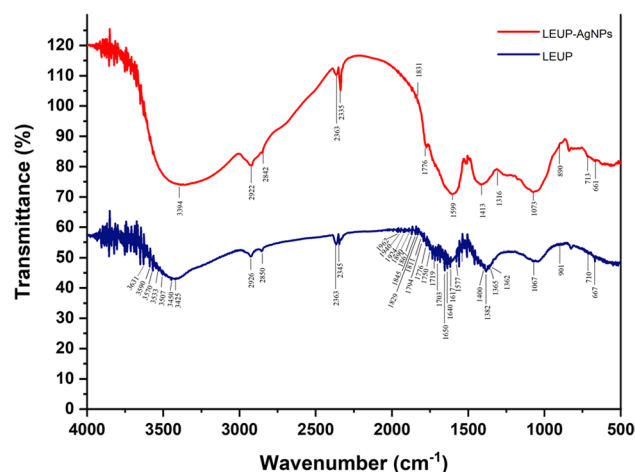


Fig. 4 FTIR spectra of LEUP, and bio-based synthesized LEUP-AgNPs

was associated with the 1067 cm^{-1} , 901 cm^{-1} , and 710 cm^{-1} bands. The band 667 cm^{-1} denoted the alcohol, O–H, out of the plane bend.

The surface chemistry or functionalization of AgNPs with specific biomolecules is also one of the factors that affect their biological properties. Through the investigation of the IR spectrum of LEUP-AgNPs, the functional group involved in their reduction process and available over their surface for cell-AgNP interactions was deduced. The phenol O–H stretch (3425 to 3631 cm^{-1}), amine (1650 cm^{-1} , 1640 cm^{-1} , 1617 cm^{-1} , and 1577 cm^{-1}), and phenol or tertiary alcohol O–H bend (1403 cm^{-1} , 1382 cm^{-1} , 1365 cm^{-1} , and 1362 cm^{-1}) bands were absent in LEUP-AgNPs [63]. These groups were present in the LEUP spectrum, as mentioned above. It indicated that the following groups of LEUP donated electrons to Ag^+ to form Ag^0 and stabilized LEUP-AgNPs [64]. Phenolic compounds absorbed photons, got excited, and reduced AgNPs [51]. As amines were present in the LEUP, it might have contained a protein that assisted in stabilizing and encapsulating LEUP-AgNPs [65]. The OH group of the phenol or tertiary alcohol donated an electron to reduce Ag^+ into Ag^0 . The 5-membered ring anhydride band (1867 cm^{-1}) of LEUP shifted to 1831 cm^{-1} in LEUP-AgNPs. The secondary amine, NH bend 1617 cm^{-1} of LEUP shifted to 1599 cm^{-1} in LEUP-AgNPs. The C–C vibration peaks 1067 cm^{-1} , 901 cm^{-1} , and 710 cm^{-1} of LEUP shifted to 1073 cm^{-1} , 890 cm^{-1} , and 713 cm^{-1} in LEUP-AgNPs. The alcohol OH out of the plane band (667 cm^{-1}) of LEUP shifted to 661 cm^{-1} in LEUP-AgNPs, respectively. The IR spectrum of LEUP-AgNPs exhibited a group frequency of 3394 cm^{-1} assigned to the NH stretch of the primary aliphatic amine. The carboxylate group peak belonged to 1413 cm^{-1} . The aromatic primary amine peak was attributed to 1316 cm^{-1} . The surface functionalization

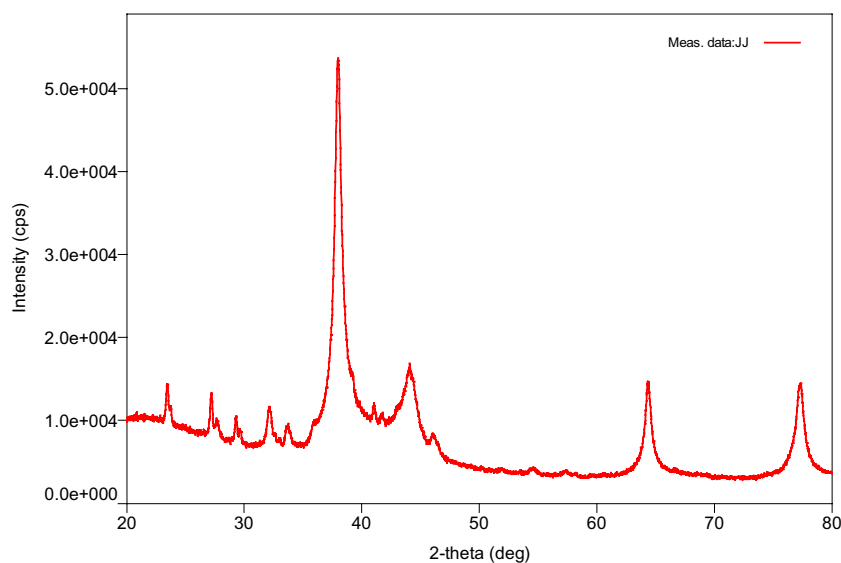
of LEUP-AgNPs consisted of a neutral alcohol (–OH) group, a positive amine (R_2NH_2), and a negative carboxyl (–COOH) group. The presence of more amine raised the magnitude of the positive surface charge and enhanced their interaction and penetration into the cell [66], which would have a net negative charge over their cell membrane.

The analysis revealed that both LEUP and LEUP-AgNPs contained methylene C–H asymmetrical or symmetrical stretch (2849 cm^{-1}), C≡N stretch of nitrile (2363 cm^{-1} and 2345 cm^{-1}), and aryl carbonate (1776 cm^{-1}) band. Since there is no difference in the group frequencies of LEUP and LEUP-AgNPs, it may be concluded that these groups did not interact with silver cations in the LEUP-AgNPs reduction reaction.

3.3.2 XRD of LEUP-AgNPs

The XRD pattern showed four characteristic peaks for the LEUP-AgNPs (Fig. 5). The bands obtained at 2θ values 37.95° , 44.14° , 64.32° , and 77.16° (Table S1) conform to Bragg's reflections at 111, 200, 220, and 311 [42]. These band values correspond to the peak values of JCPDS file 00–004–0783 of Ag. The calculated lattice constant of LEUP-AgNPs formed was 4.09 \AA . It was close to the standard lattice constant (4.08 \AA). This stated that the LEUP-AgNPs had face-centered cubic lattices [67]. The average crystallite size (D) of LEUP-AgNPs was 13.60 nm . The stability of nanoparticles is significantly affected by how closely the computed lattice constant resembles the standard value for face-centered cubic (FCC) lattices. A deviation from the reference value pointed to structural defects in the lattice, which could affect the nanoparticles' overall stability and behaviour, such as their mechanical, optical, and electronic properties [68]. These nanoparticles' well-researched

Fig. 5 X-ray diffraction pattern of LEUP-AgNPs



structural characteristics make them appropriate for both domestic and commercial applications, including catalysis, imaging, medicines, and environmental and sustainable uses [69].

3.3.3 HR-TEM and SAED of LEUP-AgNPs

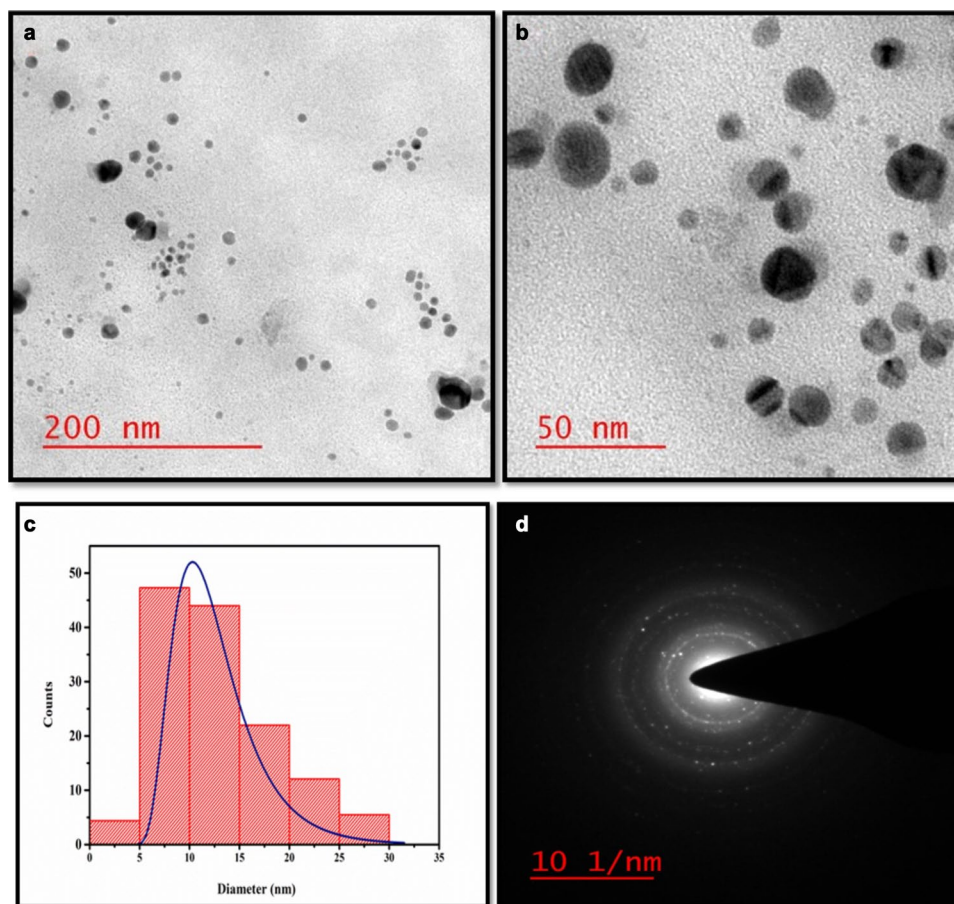
The TEM images showed LEUP-AgNPs structures at 200 nm (Fig. 6a) and 50 nm (Fig. 6b) scales. Biosynthesized LEUP-AgNPs were circular and evenly distributed [70]. The particle size distribution histogram of fabricated LEUP-AgNPs revealed that the maximum diameter of LEUP-AgNPs was 4.68–35.8 nm (Fig. 6c). The average diameter of LEUP-AgNPs was 13.04 ± 5.97 nm. The SAED pattern showed the presence of a bright ring, which confirmed the crystalline nature of LEUP-AgNPs (Fig. 6d). Based on the nucleation and growth theory of nanoparticles, the duration of nanoparticle synthesis is one of the chief factors in evaluating the shape and size distribution of the nanoparticle. If a silver nanoparticle formed with in a short duration, it would have a small size and narrow size distribution. The optimal LEUP-AgNPs synthesis occurred after 30 min of sunlight irradiation (Fig. S2). The small and narrow size distribution of LEUP-AgNPs is shown in Fig. 6b and Fig. 6c.

A literature survey revealed that the size distribution and morphology of nanoparticles are two of the major physico-chemical properties involved in nanoparticles' interactions with the biological system and subsequently impact their biological activity. Nanoparticles with smaller sizes and different shapes typically exhibit greater cellular uptake and penetration, potentially leading to enhanced bioavailability and therapeutic efficacy. This is supported by investigations such as that conducted by [71], which demonstrated the size-dependent adsorption, cellular uptake, and haemolytic activity of nanoparticles. Stoehr et al. showed that different types of nanoparticle shapes, such as nanospheres and nanowires had different impact on human alveolar epithelial cells [72].

3.3.4 HR-SEM and EDX of LEUP-AgNPs

The SEM images (Fig. 7a and 7b) showed LEUP-AgNPs structures at 400 nm and 200 nm, respectively. LEUP-AgNPs were quasi-spherical [73]. The diameter of LEUP-AgNPs was 8–20 nm. The average LEUP-AgNPs size determined by ImageJ was 13.19 ± 0.69 nm (Fig. 7c). The calculated polydispersity of LEUP-AgNPs was 9.4%. The existence of silver in the fabricated LEUP-AgNPs was demonstrated by the electron dispersive X-ray map (Fig. 7d) and its overlay

Fig. 6 HR-TEM images of LEUP-AgNPs. (a) at 200 nm. (b) at 50 nm. (c) Particle size distribution of LEUP-AgNPs. (d) SAED patterns of LEUP-AgNPs



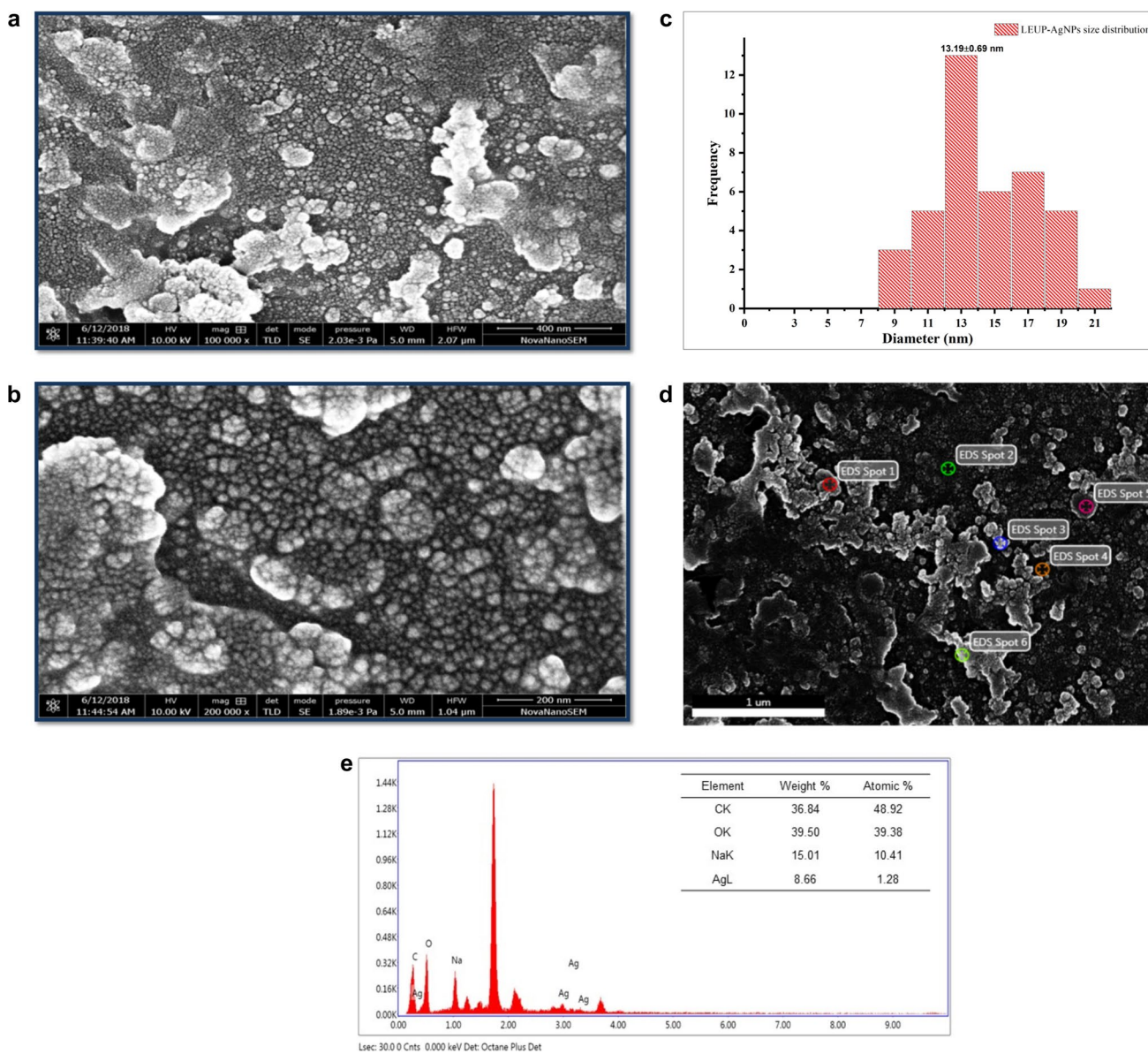


Fig. 7 HR-SEM images of LEUP-AgNPs. **(a)** at 400 nm. **(b)** at 200 nm. **(c)** Particle size distribution of LEUP-AgNPs. **(d)** EDX element mapping showing presence of Ag, O, Na, and C in LEUP-AgNPs. **(e)** Electron dispersive X-ray analysis of LEUP-AgNPs

(Fig. S6). The formation of a prominent band between 3 and 4 keV showed the existence of Ag and revealed its crystalline nature (Fig. 7e). The LEUP-AgNPs also contained elements like carbon and oxygen, indicating the presence of biomolecules adhered to the LEUP-AgNPs. Silica and sodium element peaks were observed because the LEUP-AgNPs were coated over the glass.

3.3.5 AFM of LEUP-AgNPs

The topographical properties of synthesized LEUP-AgNPs were studied through their 2D (Fig. 8a) and 3D (Fig. 8b) images generated by AFM. After analysis, the calculated

mean roughness of LEUP-AgNPs was 7.68 nm. The LEUP-AgNPs roughness profile revealed that the maximum peak height was 25.8 nm and the maximum valley depth was 20.6 nm, respectively (Fig. 8c). Singh et al. reported similar findings regarding silver nanoparticle roughness profiles [74].

3.3.6 DLS of LEUP-AgNPs

The LEUP-AgNPs orientation generated speckle patterns. The continuous variation in LEUP-AgNPs movement altered the speckle patterns with respect to time. DLS detected the fluctuation in speckle pattern on the time scale and measured

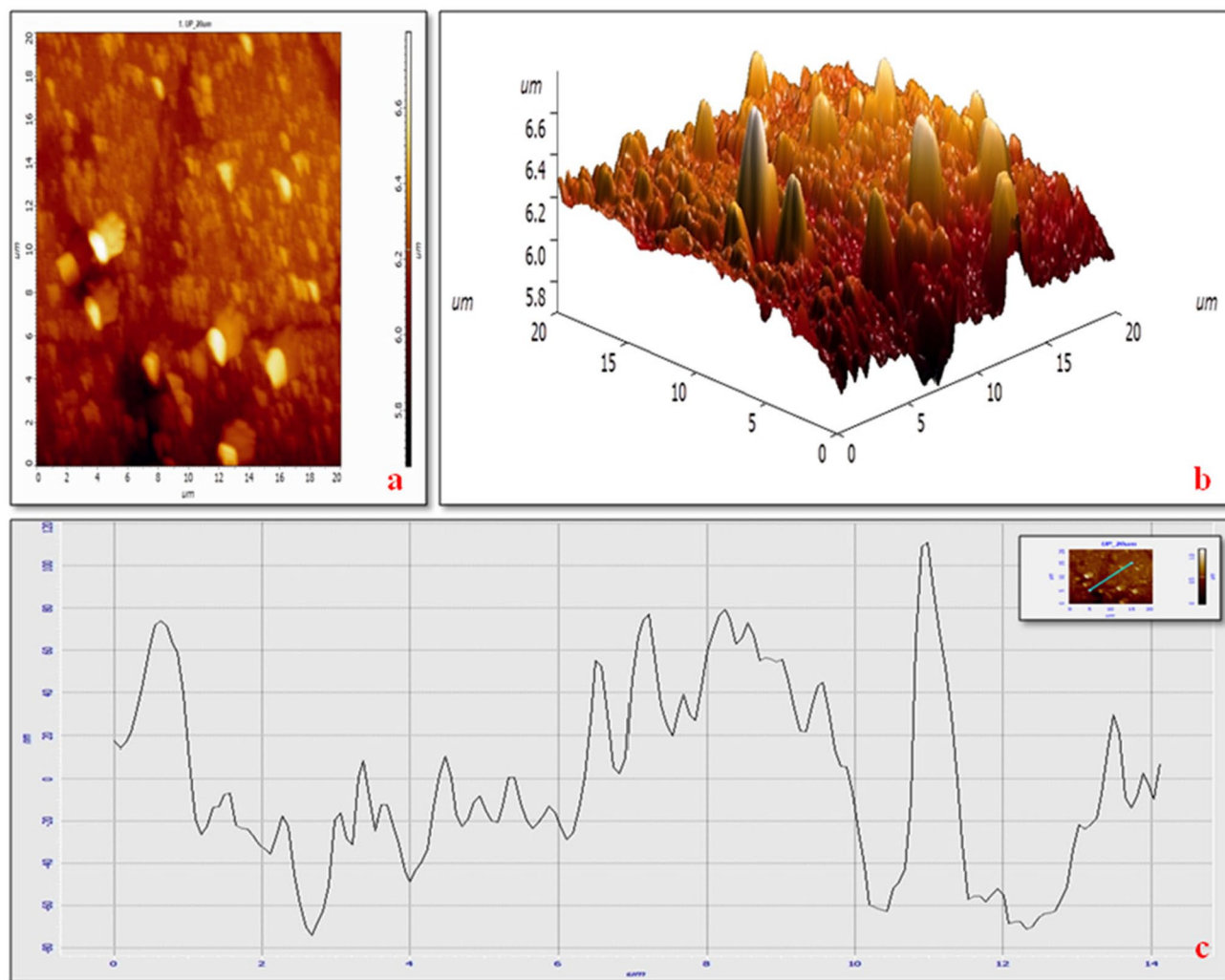


Fig. 8 AFM images of LEUP-AgNPs. **(a)** 2D image. **(b)** 3D image. **(c)** Roughness profile histogram of LEUP-AgNPs

the quantitative light scattering intensity of LEUP-AgNPs. The change in light scattering intensity was expressed as the intensity correlation function $G_2(\tau)$. Tau (τ) was a symbol for the lag time between two-time points. The graph $\ln(G_2(\tau)-1)$ vs. τ (Fig. 9a) showed that $G_2(\tau)$ of LEUP-AgNPs possessed an exponential decay. The LEUP-AgNPs diffused slowly with respect to time. Hence, $G_2(\tau)$ decayed at a slower rate. The $G_2(\tau)$ defined diffusion behaviours such as diffusion constant, hydrodynamic radii, and homogeneity of LEUP-AgNPs. The cumulants' results were obtained from $G_2(\tau)$ fitting through a monomodal distribution approach. The diffusion constant (D) of LEUP-AgNPs was $5.151 \times 10^{-8} \text{ cm}^2 \text{ sec}^{-1}$. The hydrodynamic diameter (d) of LEUP-AgNPs was 95.5 nm. The polydispersity index (γ) of LEUP-AgNPs was 0.2 [75]. If $\gamma \geq 0.1$, the particles were highly monodisperse. If $\gamma = 0.1-0.7$, the particles were nearly monodisperse. The particles were polydisperse if $\gamma > 0.7$. Hence, the LEUP-AgNPs were nearly monodisperse [60]. The CONTIN

(constrained regularization method for inverting data) results were evaluated from $G_2(\tau)$ fitting through the non-monomodal distribution method (Fig. 9a). It showed that the finite numbers of LEUP-AgNPs were distributed away from the average hydrodynamic diameter. The LEUP-AgNPs diameters estimated through the intensity distribution curve (Fig. 9b), volume distribution curve (Fig. 9c), and number distribution curve (Fig. 9d) were 123.9 ± 64.6 , 64.3 ± 28.5 , and 47.5 ± 12.9 nm, respectively.

3.3.7 Zeta potential of LEUP-AgNPs

The potential drop at the electric double layer around the LEUP-AgNPs was measured through the Zetasizer Nano ZS. The LEUP-AgNPs exhibit a -17.8 mV electrostatic potential (Fig. 10). The negative sign indicates the anionic behaviour of LEUP-AgNPs [76]. Due to the negative charge, LEUP-AgNPs would repel each other and avoid

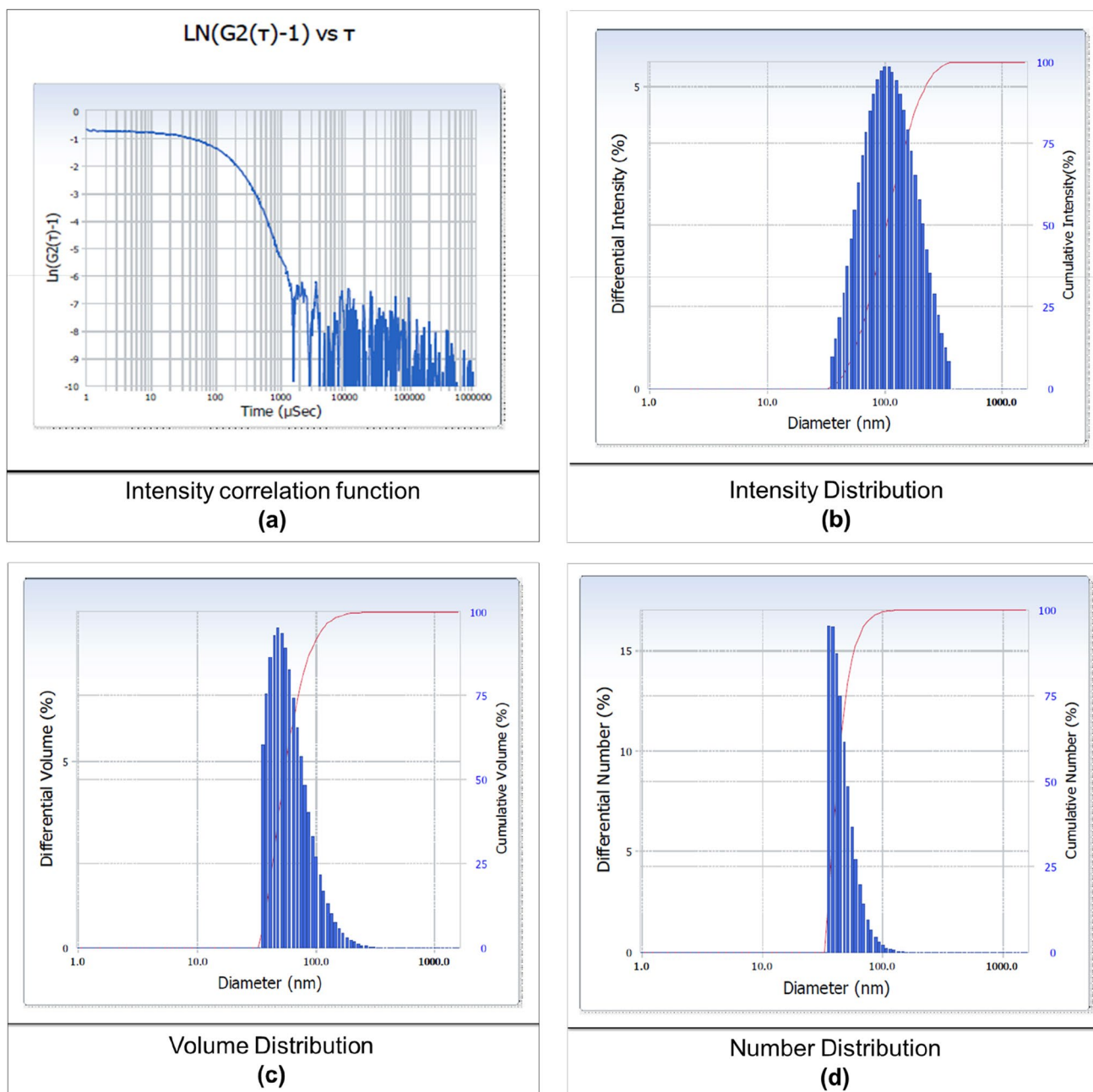


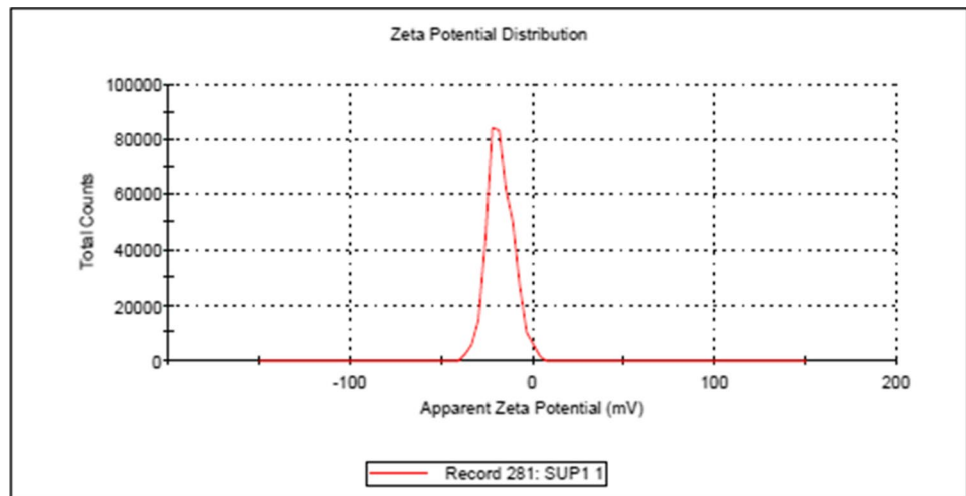
Fig. 9 LEUP-AgNPs analysis through dynamic light scattering. (a) Intensity correlation function. (b) Intensity distribution. (c) Volume distribution. (d) Number distribution

agglomeration. It pointed towards the LEUP-AgNPs' stability. AgNPs with zeta potential greater than or equal to 30 mV or less than -30 mV are indicative of a stable system. The type and magnitude of surface charge of AgNPs depend on the reducing agent of their fabrication reaction and affect their biological effects. The lower magnitude of negative zeta potential reduced the electrostatic barrier and increased the probabilities of cell-particle interactions with cell surfaces having a net negative charge and promoting higher toxicity [77].

3.3.8 XPS of LEUP-AgNPs

The XPS technique was utilized to acquire details regarding the compositions, electronic configuration, and oxidation states of the LEUP-AgNPs surface. The XPS graph of LEUP-AgNPs demonstrated the binding energy of electrons (1–1300 eV) concerning electron counts per second (Fig. 11a). The four characteristic peaks of distinct binding energy represent the presence of oxygen (O), nitrogen (N), silver (Ag), and carbon (C) on the LEUP-AgNPs surface.

Fig. 10 Zeta potential of LEUP-AgNPs



The peak at 532.11 eV binding energy reflected the photoelectron emission from the 1 s orbital of O (Fig. 11b). The formation of a peak at 406.68 eV binding energy indicated the photoelectron emission from the 1 s orbital of N (Fig. 11c). The occurrence of two characteristic peaks at 368.3 and 374.4 eV binding energies (Fig. 11d) corresponded to the emission of electrons from Ag 3d_{5/2} and Ag 3d_{3/2}, respectively [78]. The binding energy peak at 285.03 eV confirmed the emission of electrons from the 1 s orbital of C (Fig. 11e).

3.4 Antioxidant activity of LEUP-AgNPs

The LEUP-AgNPs (100 µg mL⁻¹) showed 17.3% inhibition of DPPH free radicals. The highest LEUP-AgNPs concentration (1000 µg mL⁻¹) scavenged maximum DPPH free radicals, i.e., 69.5% ($p \leq 0.05$). A directly proportional relation between LEUP-AgNPs concentration and DPPH free radical inhibition was observed (Fig. 12) [79]. The LEUP-AgNPs IC₅₀ of 709.76 µg mL⁻¹ was close to the ascorbic acid IC₅₀ of 457.91 µg mL⁻¹. It indicated that the LEUP-AgNPs (IC₅₀ 709.76 µg mL⁻¹) improved the antioxidant potential of LEUP (IC₅₀ 2666.95 µg mL⁻¹). A similar finding was reported for *Virola oleifera*-capped gold nanoparticles. AgNPs' antioxidant activity was increased by a change in the phytochemicals' electron concentration over the surface of the nanoparticle [80].

3.5 Anti-promastigote activity of LEUP-AgNPs

The anti-promastigote inhibitory effect of LEUP and LEUP-AgNPs was studied under in vitro conditions. Growth inhibitory effects of LEUP (1.5–200 µg mL⁻¹) and LEUP-AgNPs (1.5–200 µg mL⁻¹) were studied against promastigotes. The number of viable promastigotes decreased with an increase in silver nanoparticles and leaf extract concentration. It was

observed that the per cent inhibition of the growth of promastigotes was inversely correlated with the dose of LEUP and LEUP-AgNPs [81]. The LEUP's highest concentration, 200 µg mL⁻¹, inhibited fifty-three percent of promastigotes' growth (Table 1). The LEUP-AgNPs' highest concentration, 200 µg mL⁻¹, inhibited sixty-eight percent of promastigotes growth (Table 1). The LEUP-AgNPs showed better percent of growth inhibition in promastigotes.

A literature survey supported the idea that promastigotes are 15–25 µm × 1.5–3.5 µm in size. One nucleus and a flagellum are visible in them (Fig. 13a). The visual investigation of promastigotes under microscopy showed that miltefosine treatment caused the loss of flagella and the circularization of promastigotes (Fig. 13b). The LEUP and LEUP-AgNPs induced cytoplasmic condensation, shrinkage, size reduction, and aggregations of promastigotes (Figs. 13c and d). In comparison with LEUP, LEUP-AgNPs showed more pronounced effects on the cell morphology and high death profile of promastigotes. The IC₅₀ value was used to express the anti-promastigotes activity of LEUP and LEUP-AgNPs. The LEUP IC₅₀ for the promastigotes stage was determined to be 47.90 µg mL⁻¹. *Embilica officinalis*, *Putranjiva roxburghii*, and *Corchorus capsularis* extracts checked the promastigote's growth with IC₅₀ values of 21.6, 25.6, and 79.0 µg mL⁻¹, respectively [38–40]. The LEUP-AgNPs IC₅₀ value for promastigotes was 6.72 µg mL⁻¹ which was considerably ($P < 0.001$) less than the LEUP IC₅₀ value. The LEUP-AgNPs IC₅₀ of 6.72 µg mL⁻¹ was close to the miltefosine IC₅₀ of 7.20 µg mL⁻¹ (Table 2). It indicated that LEUP-AgNPs had enhanced the anti-leishmanial property of *U. picta* based on the IC₅₀ value. The LEUP-AgNPs were smaller (13 nm) and had a much more efficient IC₅₀ of 6.72 µg mL⁻¹ when compared with the subsequently published nanoparticles [41, 42, 44, 58]. With an IC₅₀ value of 23.4 µM, arsenic nanoparticles prevented promastigotes

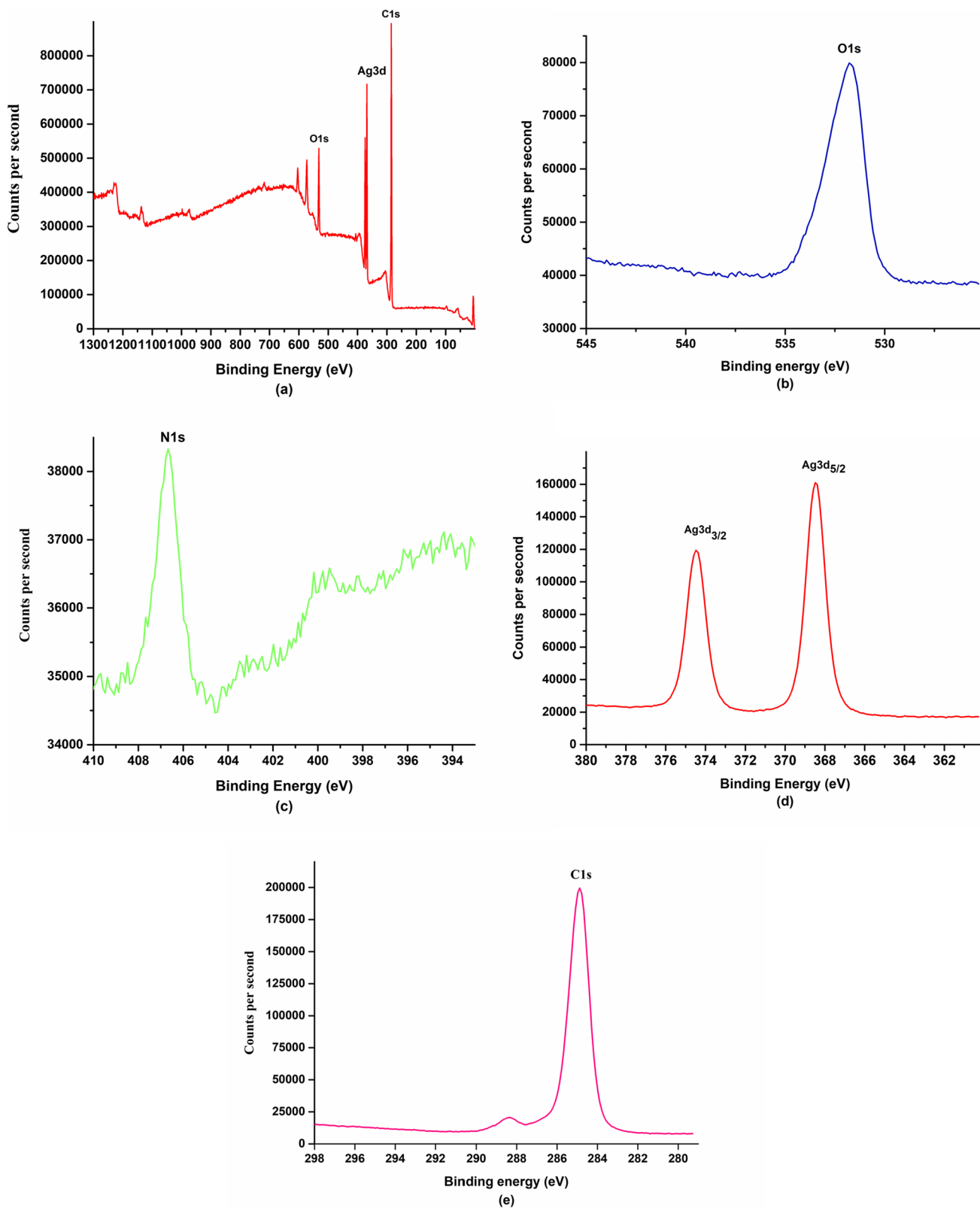


Fig. 11 X-ray photoelectron spectroscopy of LEUP-AgNPs. **(a)** Wide scan spectrum of LEUP-AgNPs. **(b)** Specific scan spectrum of O (*1 s*) region. **(c)** Specific scan spectrum of N (*1 s*) region. **(d)** Specific scan spectrum of Ag (*3d*) region. **(e)** Specific scan spectrum of C (*1 s*) region

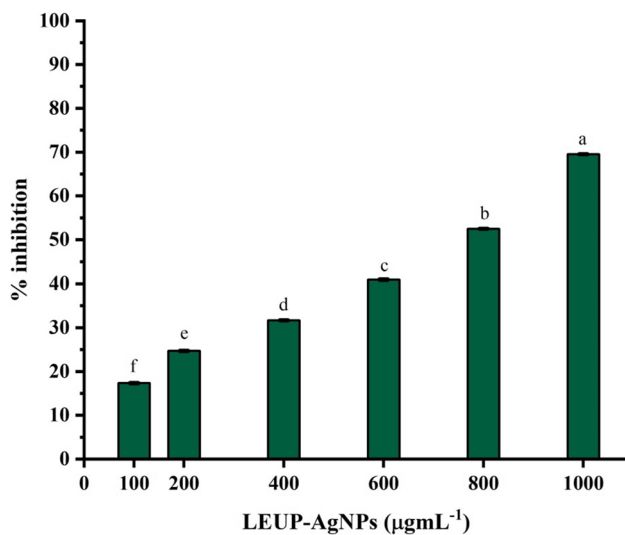


Fig. 12 Antioxidant activity of LEUP-AgNPs. Data is expressed as mean \pm S.E. The statistical significance difference in data analysed by one way analysis of variance (ANOVA) followed by post hoc Tukey's b test. The alphabetical letters a-f indicates significant difference between the concentrations (at $p < 0.05$)

from proliferating [82]. The 12 nm AgNPs synthesized using *Euphorbia prostrata* suppressed leishmania cell proliferation with an IC_{50} of $14.94 \mu\text{g mL}^{-1}$ [41]. The $Au_{\text{core}} Ag_{\text{shell}}$ nanoparticles synthesized using *Dioscorea bulbifera* ($32 \mu\text{g mL}^{-1}$) demonstrated minimum inhibition of promastigotes growth [58]. The 18 nm AgNPs biosynthesized using *Xanthium strumarium* leaf extract inhibited promastigotes growth of *L. donovani* with an IC_{50} value of $8.93 \mu\text{g mL}^{-1}$ [42]. Phytofabricated silver nanoparticles synthesized through *Secchium edule* checked the promastigotes' growth with an IC_{50} of $51.88 \mu\text{g mL}^{-1}$ [43]. 7, 8-dihydroxyflavone functionalized gold nanoparticles IC_{50} was $40 \mu\text{M}$ against the promastigotes stage [44].

According to the literature survey, the multiplication of both life stages of *L. donovani* was associated with their pH homeostasis. The promastigotes maintain intracellular pH at neutral and extracellular pH at 5–7.4. Active transport of substrates across the cell membrane requires a positive pH gradient to extracellular pH. Reported literature suggested that promastigotes' acidic extracellular environment facilitated the release of Ag^+ and phytoconstituents from bio-based synthesized AgNPs [83]. The Ag^+ ions and phytoconstituents caused oxidative injuries to the cell membrane and disturbed intracellular pH. Consequently, increased production of intracellular oxygen-free radicals induced a respiratory burst mechanism, altered the chemical structure of DNA, and resulted in apoptosis [26]. A *L. donovani* cell consists of only one mitochondrion, which is necessary for survival. Reactive oxygen species (ROS) damage the respiratory system present in mitochondria and cause death. The apoptosis signaling pathway is one of the identified mechanisms of promastigote-stage killing carried on by the biosynthesized AgNPs. Phosphatidylserine, an apoptotic biomarker, is only present on the cytoplasmic side of the cell membrane. The apoptosis-inducing factors provoke phosphatidylserine to come up on the exterior layer of the cytoplasmic membrane. Phagocytes recognize the biomarker and stimulate the ingestion of post-apoptotic cell debris [84]. According to the literature on anti-leishmanial activity, it was clear that more studies had focused on the promastigotes stage of *L. donovani* and had not been done on the amastigotes stage of the parasite.

3.6 Effects of LEUP-AgNPs on intra-macrophage amastigotes

The current experiment examined how LEUP and LEUP-AgNPs affected the pathogen's amastigotes stage. The results showed that $1.5 \mu\text{g mL}^{-1}$ of LEUP and LEUP-AgNPs

Table 1 Effects of LEUP and bio-based synthesized LEUP-AgNPs on per cent growth inhibition of *L. donovani* promastigote form and intra-RAW 264.7 macrophage amastigotes form of *L. donovani*

Concentration ($\mu\text{g mL}^{-1}$)	% Growth inhibition (Mean \pm S.E.)			
	Promastigote form		Intra-RAW 264.7 macrophage amastigotes form	
	LEUP	LEUP-AgNPs	LEUP	LEUP-AgNPs
1.5	39.52 ± 1.14	38.82 ± 0.69	31.50 ± 1.50	$51.00 \pm 1.00^*$
3.125	41.08 ± 0.89	42.99 ± 0.16	$36.00 \pm 1.00^*$	$55.50 \pm 1.50^{**}$
6.25	43.20 ± 0.76	$48.34 \pm 0.72^{***}$	$39.50 \pm 1.50^{**}$	$58.00 \pm 2.00^{**}$
12.5	44.51 ± 0.50	$50.98 \pm 0.91^{***}$	$44.00 \pm 1.00^{***}$	$62.00 \pm 2.00^{***}$
25	46.02 ± 0.84	$53.99 \pm 0.93^{***}$	$46.00 \pm 1.00^{***}$	$66.50 \pm 1.50^{***}$
50	$50.04 \pm 1.86^*$	$58.24 \pm 0.94^{***}$	$49.00 \pm 1.00^{***}$	$71.00 \pm 1.00^{***}$
100	$51.86 \pm 1.07^{**}$	$66.27 \pm 0.42^{***}$	$51.00 \pm 1.00^{***}$	$76.00 \pm 1.00^{**}$
200	$53.17 \pm 1.22^{***}$	$68.04 \pm 0.90^{***}$	$53.00 \pm 1.00^{***}$	$80.00 \pm 2.00^*$

Data is expressed as mean \pm S.E. The symbol * indicates significant difference between the concentrations (at $p < 0.001$)

Fig. 13 Morphological differences observed in promastigotes form of *L. donovani* (a) Untreated. (b) Miltefosine. (c) LEUP. (d) LEUP-AgNPs treated. The blue arrows mark circularization and loss of flagella and black arrows mark cytoplasmic condensation, shrinkage, size reduction and aggregation of cells

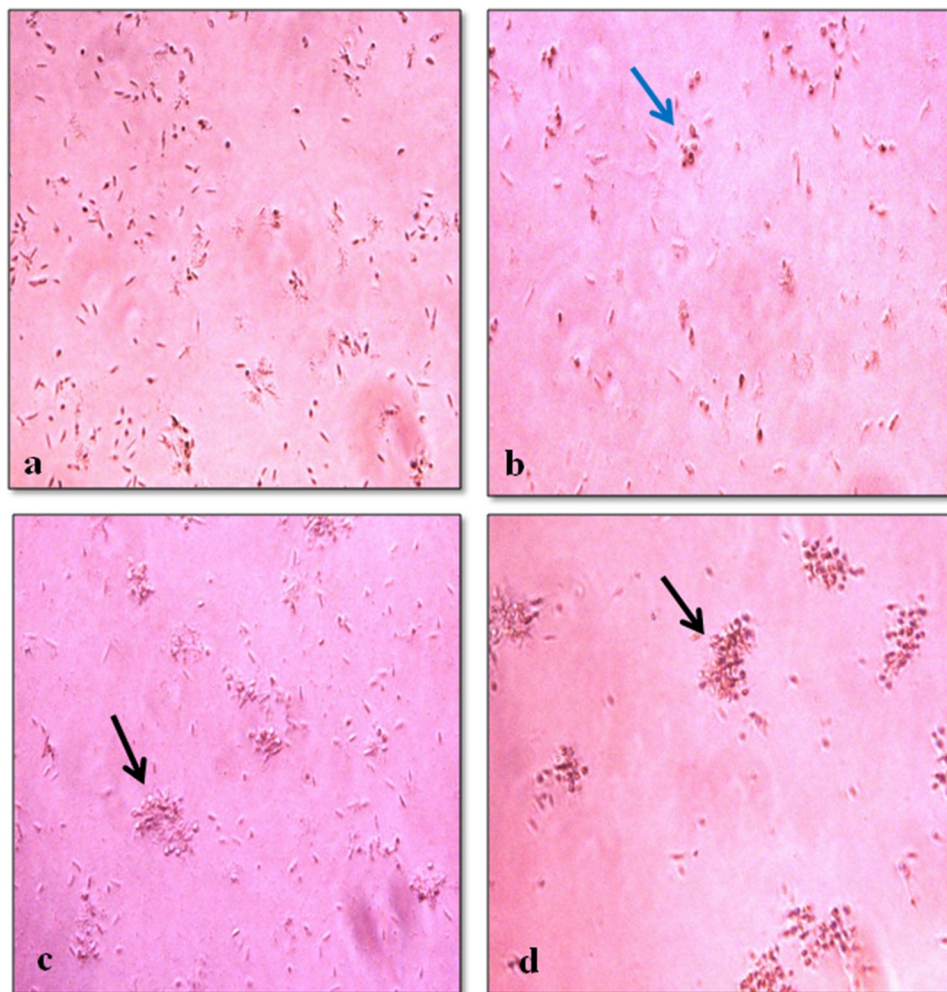


Table 2 Anti-leishmanial and cytotoxic activity of LEUP and LEUP-AgNPs

Sample	^a IC ₅₀ for <i>L. donovani</i> form ($\mu\text{g mL}^{-1}$)		^b CC ₅₀ on RAW 264.7 macrophage ($\mu\text{g mL}^{-1}$)	^c SI of intra- macrophage amastigotes form
	Promastigotes	Intra-macrophage amastigotes		
LEUP	47.90	28.97	< 200	6.90
LEUP-AgNPs	6.72	1.16	< 200	172.41
Miltefosine	7.20	8.10	< 100	12.34

^aIC₅₀ is half-maximal inhibitory concentration of sample for *L. donovani*

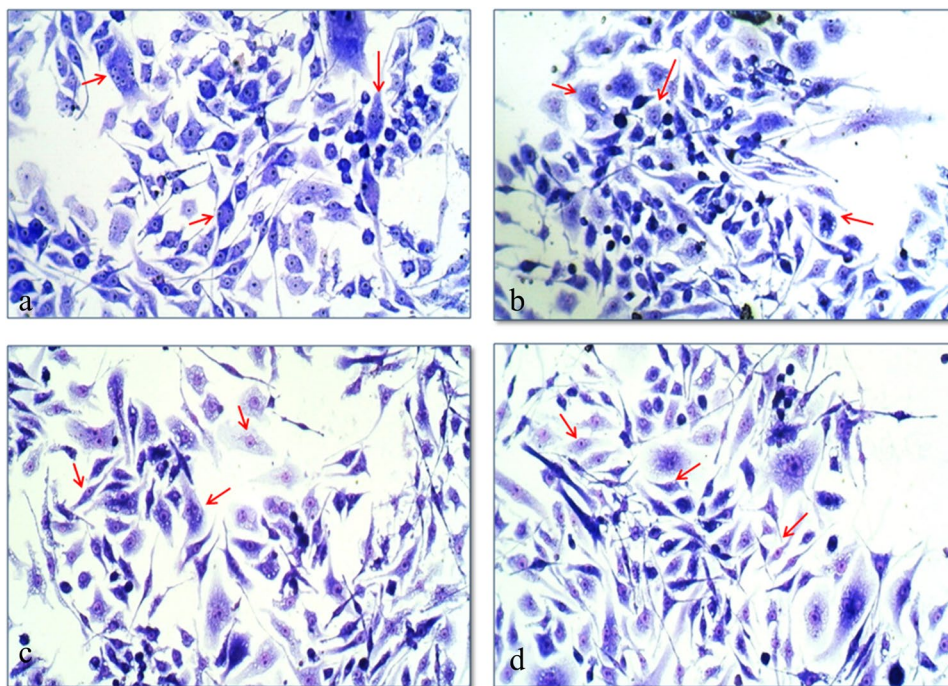
^bCC₅₀ is used to measure toxicity. It is the concentration that reduces the multiplication of RAW264.7 macrophages up to 50%

^cSelectivity index (SI) is the ratio of CC₅₀ in RAW cells and IC₅₀ in intracellular amastigotes form

induced a minimum percent inhibition of amastigotes growth (Table 1). With an increase in LEUP and LEUP-AgNPs concentrations ($1.5\text{--}200\ \mu\text{g mL}^{-1}$), the percentage of amastigotes growth inhibition was also increased. It indicated the LEUP and LEUP-AgNPs exhibited dose-dependent amastigotes growth inhibition relations [85]. Fifty-three percent growth inhibitions were found to be associated with $200\ \mu\text{g mL}^{-1}$

of LEUP (Table 1). However, eighty percent of intracellular amastigotes were suppressed by the highest dose of LEUP-AgNPs, $200\ \mu\text{g mL}^{-1}$ (Table 1) [86]. In comparison with the untreated intra-RAW264.7 macrophages (Fig. 14a), there was a decrease in the number of amastigotes present inside RAW 264.7 macrophages treated with miltefosine (Fig. 14b), LEUP (Fig. 14c), and LEUP-AgNPs (Fig. 14d).

Fig. 14 Morphological differences observed in intra-RAW 264.7 macrophage amastigotes form of *L. donovani*. **(a)** Untreated. **(b)** Miltefosine. **(c)** LEUP. **(d)** LEUP-AgNPs. The red arrow mark number of amastigotes per intra-RAW 264.7 macrophage



Miltefosine killed or induced the apoptosis-like death of intracellular amastigote. The anti-intracellular amastigote activity of LEUP and LEUP-AgNPs was expressed as IC_{50} . The LEUP showed growth inhibition activity against the amastigotes stage within macrophages with an IC_{50} of $28.97 \mu\text{g mL}^{-1}$. However, the 13 nm LEUP-AgNPs inhibited the amastigotes stage in RAW264.7 macrophages with an IC_{50} of $1.16 \mu\text{g mL}^{-1}$. The IC_{50} of LEUP-AgNPs ($1.16 \mu\text{g mL}^{-1}$) was significantly more effective than the LEUP IC_{50} ($28.97 \mu\text{g mL}^{-1}$) and miltefosine IC_{50} ($8.10 \mu\text{g mL}^{-1}$) (Table 2). The results revealed that the LEUP-AgNPs showed more growth inhibitory effects against *L. donovani* intra-macrophage amastigotes than LEUP. The fabrication of LEUP-AgNPs from the leaf extract enhanced the anti-leishmanial action. A literature survey revealed that *Leishmania* parasites enter macrophages and establish themselves in the parasitophorous vacuoles (PVs). The PVs maintain the infection in the amastigote stage and guard it against the defence mechanisms of macrophages [87]. According to reports, prevention of ROS generation is one defence mechanism that intracellular *Leishmania* infection uses against host macrophages. The NADPH oxidase enzyme in the phagosome and cell membrane produces superoxide radicals. These reactive oxygen species kill intracellular microorganisms. *Leishmania* parasites are sensitive to ROS. *Leishmania* infection inhibits the establishment of NADPH oxidase complex assembly on the *Leishmania* parasitophorous vacuole membrane [88]. The generation of oxidative stress might induce antioxidant enzymes and cellular events like cell cycle arrest, apoptosis, and inflammation.

3.7 Cytotoxic effects of LEUP and LEUP-AgNPs on RAW264.7 macrophages

The cytotoxic activity of LEUP and LEUP-AgNPs was expressed as CC_{50} against RAW264.7 macrophages (Table 2). The CC_{50} of LEUP and LEUP-AgNPs was less than $200 \mu\text{g mL}^{-1}$ on the macrophage. The CC_{50} of miltefosine was less than $100 \mu\text{g mL}^{-1}$ [89]. The cytotoxicity activity of miltefosine was significantly higher against RAW264.7 macrophages with respect to LEUP and LEUP-AgNPs. The LEUP-AgNPs and LEUP did not induce cytotoxicity in RAW264.7 macrophages. Based on the results of the current investigation, LEUP-AgNPs showed efficient anti-promastigote and intra-macrophage amastigote activities without causing any cytotoxicity in RAW264.7 macrophages. The findings provide hope for nanomedicine against *L. donovani* after an in-depth clinical evaluation.

4 Conclusion

The bio-based silver nanoparticles were synthesized with a size-controlled distribution by using *U. picta* leaf extract. The nanoparticles were optimized based on photoperiod, inoculum, silver salt molarity, and pH factor. The biomolecules from the extract served as stabilizing, functionalizing, and reducing agents on the surface of the nanoparticles. The FTIR showed that nanoparticles were encapsulated with *U. picta* extract. The biomolecules in the extract changed the nanoparticle surface's electric potential from a negative

charge to a positive one. The bio-based silver nanoparticles possessed higher free radical scavenging potential than *U. picta* extract. The particles were rough and had a high surface area per unit volume on account of the binding of phytoconstituents around the silver ions. The characteristic structural features of bio-based synthesized silver nanoparticles promote their utility against various pathological conditions. The silver nanoparticles significantly inhibited the promastigotes and amastigotes forms of *L. donovani*, which cause visceral leishmaniasis. The bio-based particles did not exhibit cytotoxic properties against RAW264.7 macrophages. It suggested the application of *U. picta* and its bio-based silver nanoparticles for the treatment of visceral leishmaniasis after an in-depth evaluation.

Supplementary Information The online version contains supplementary material available at <https://doi.org/10.1007/s13399-024-05736-6>.

Acknowledgements The authors acknowledge all the necessary instrumentation facilities provided by the Head, Department of Botany, MMV, Banaras Hindu University, Varanasi and IIT-BHU, Varanasi. Author Kavindra Nath Tiwari thankfully acknowledges Banaras Hindu University, Varanasi for providing financial assistance through an incentive grant under the Institutions of Eminence (IoE) scheme (6031) for research.

Author contribution Conceptualization, Methodology, Formal analysis, Validation, Formal analysis, Investigation, Data curation, Writing-original draft, Editing, Visualization: [Jyoti Dixit]; Plant material collection, Sample preparation: [Pradeep Kumar]; Investigation, Formal analysis: [Rajan Singh]; Investigation, Formal analysis: [Pooja Verma]; Conceptualization, Validation, Resources, Writing-review, Supervision: [Kavindra Nath Tiwari]; Investigation, Resources: [Rakesh Kumar Singh]; Resources: [Sunil Kumar Mishra]; Resources: [Jasmeet Singh].

Funding The research did not receive any specific grant from funding agencies.

Declarations

Ethical approval Not applicable.

Consent to participate Not applicable.

Consent for publication Not applicable.

Competing interest The authors declare no competing interest.

References

- Khare CP, (2008) Indian Medicinal Plants- An illustrated dictionary. 1st ed. Springer, New York. <https://doi.org/10.1007/978-0-387-70638-2>
- Okusanya OT, Lakanmi OO, Oyesiku OO (1991) Germination ecology of the woody herb *Uraria picta*, from Southern Nigeria. *J Trop Ecol* 7:139–146. <https://doi.org/10.1017/S0266467400005204>
- Joshi A, Yelne MB, Sharma PC, Dennis TJ (2000) Database on medicinal plants used in ayurveda, 6th ed. Central council for research in ayurveda and siddha, Deptt. of ISM & H, Ministry of Health and Family Welfare, Government of India, New Delhi
- Igboechi AC, Osazuwa EO, Igwe UE (1989) Laboratory evaluation of the acaricidal properties of extracts from *Uraria picta* (Leguminosae). *J Ethnopharmacol.* [https://doi.org/10.1016/0378-8741\(89\)90102-5](https://doi.org/10.1016/0378-8741(89)90102-5)
- Rahman MM, Gibbons S, Gray AI (2007) Isoflavanones from *Uraria picta* and their antimicrobial activity. *Phytochemistry* 68:1692–1697. <https://doi.org/10.1016/j.phytochem.2007.04.015>
- Singh S, Singh HN, Gangwar AK, Devi KS, Niyogi D, Waghaye JY (2011) Effect of *Uraria picta* on bone healing in rabbits: a radiographic, angiographic and histopathological study. *Indian J Vet Surg* 32:107–110
- Odubanjo V, Oboh G, Ibukun E (2013) Antioxidant and anticholinesterase activities of aqueous extract of *Uraria picta* (Jacq.) DC. *African J Pharm Pharmacol* 7:2768–2773. <https://doi.org/10.5897/ajpp2013.3899>
- Patel BD, Kamariya YH, Patel MB (2011) Free radical scavenging potential of ethanolic extract of *Uraria picta* LINN. *Pharmacologyonline* 2:134–145
- Garg N, Garg M, Maan AS, Sandhu BS, Mittal S, Goyal S (2012) Phytochemical studies and anti anxiety activity of *Uraria picta* leaves. *J Pharm Res Opin* 2:39–40
- Jain S, DeFilippis R (1991) Medicinal plants of India. *Med plants world* 1:1–849
- Rodrigues V, Cordeiro-da-Silva A, Laforge M, Silvestre R, Estaquier J (2016) Regulation of immunity during Visceral leishmania infection. *Parasit Vectors* 9:1–13. <https://doi.org/10.1186/s13071-016-1412-x>
- World Health Organisation (2021) The Global Health Observatory, explore a world of health data, Neglected tropical disease, Leishmaniasis. <https://apps.who.int/gho/data/node.main.NTDLEISHVEND?lang=en>
- WHO expert committee on the control of the leishmaniasis & World health organization (2010) Control of the leishmaniasis: report of a meeting of the WHO expert committee on the control of leishmaniasis, Geneva, 22–26 March 2010. <https://apps.who.int/iris/handle/10665/44412>
- Alvar J, den Boer M, Dagne DA (2021) Towards the elimination of visceral leishmaniasis as a public health problem in east Africa: reflections on an enhanced control strategy and a call for action. *Lancet Glob Heal* 9:1763–e1769. [https://doi.org/10.1016/S2214-109X\(21\)00392-2](https://doi.org/10.1016/S2214-109X(21)00392-2)
- Tiwari N, Gedda MR, Tiwari VK, Singh SP, Singh RK (2018) Limitations of current therapeutic options, possible drug targets and scope of natural products in control of leishmaniasis. *Mini Rev Med Chem* 18:26–41. <https://doi.org/10.2174/1389557517666170425105129>
- Rocha LG, Almeida JRGS, Macedo RO, Barbosa-Filho JM (2005) A review of natural products with anti-leishmanial activity. *Phytomedicine* 12:514–535. <https://doi.org/10.1016/j.phymed.2003.10.006>
- Hua S, Wu SY (2018) Editorial: Advances and challenges in nanomedicine. *Front Pharmacol* 9:1–3. <https://doi.org/10.3389/fphar.2018.01397>
- Sanchez A, Mejia SP, Orozco J (2020) Recent advances in polymeric nanoparticles-encapsulated drugs against intracellular infections. *Molecules* 25:1–45. <https://doi.org/10.3390/molecules25163760>
- Soares S, Sousa J, Pais A, Vitorino C (2018) Nanomedicine: principles, properties and regulatory issues. *Front Chem* 6:1–15. <https://doi.org/10.3389/chem.2018.00360>
- Ankamwar B (2012) Biomedical engineering-technical applications in medicine: R. Hudak (ed.), IntechOpen Limited, United Kingdom, 93–114. <https://doi.org/10.5772/46121>

21. Kumar P, Sonkar PK, Tiwari KN, Singh AK, Mishra SK, Dixit J, Ganesan V, Singh J (2022) Sensing of mercury ion using light induced aqueous leaf extract mediated green synthesized silver nanoparticles of *Cestrum nocturnum* L. *Environ Sci Pollut Res* 53:79995–80004. <https://doi.org/10.1007/s11356-022-19357-x>
22. Muthukrishnan L (2021) Multidrug resistant tuberculosis-diagnostic challenges and its conquering by nanotechnology approach-An overview. *Chem Biol Interact* 337:1–12. <https://doi.org/10.1016/j.cbi.2021.109397>
23. Jamshaid H, Din F, Khan GM (2021) Nanotechnology based solutions for anti-leishmanial impediments: A detailed insight. *J Nanobiotechnology* 19:1–51. <https://doi.org/10.1186/s12951-021-00853-0>
24. Saravanan A, Kumar PS, Karishma S, Vo Dai-Viet N, Jeevanantham S, Yaashikaa PR, George CS (2021) A review on biosynthesis of metal nanoparticles and its environmental applications. *Chemosphere* 264:1–16. <https://doi.org/10.1016/j.chemosphere.2020.128580>
25. Desireddy A, Conn BE, Guo J, Yoon B, Barnett RN, Monahan BM, Kirschbaum K, Griffith WP, Whetten RL, Landman U, Bigioni TP (2013) Ultrastable silver nanoparticles. *Nature* 501:399–402. <https://doi.org/10.1038/nature12523>
26. Ahmed S, Ahmad M, Swami BL, Ikram S (2016) A review on plants extract mediated synthesis of silver nanoparticles for antimicrobial applications: A green expertise. *J Adv Res* 7:17–28. <https://doi.org/10.1016/j.jare.2015.02.007>
27. Iravani S, Korbekandi H, Mirmohammadi SV, Zolfaghari B (2014) Synthesis of silver nanoparticles: chemical, physical and biological methods. *Res. Pharm. Sci.* 9:385–406
28. Gentile C (2021) Biological activities of plant food components: implications in human health. *Foods* 10(456):1–2. <https://doi.org/10.3390/foods10020456>
29. Asif M, Yasmin R, Asif R, Ambreen A, Mustafa M, Umbreen S (2022) Green Synthesis of silver nanoparticles (AgNPs), structural characterization, and their antibacterial potential. *Dose-Response* 20:1–11. <https://doi.org/10.1177/15593258221088709>
30. Bernela M, Seth M, Kaur N, Sharma S, Pati PK (2023) Harnessing the potential of nanobiotechnology in medicinal plants. *Ind Crops Prod* 194(116266):1–17. <https://doi.org/10.1016/j.indcrop.2023.116266>
31. Viswanathan S, Palaniyandi T, Shanmugam R, Pandi SKM, Wahab MRA, Baskar G, Rajendran BK, Sivaji A, Moovendhan M (2024) Synthesis, characterization, cytotoxicity, and antimicrobial studies of green synthesized silver nanoparticles using red seaweed *Champia parvula*. *Biomass Convers Biorefn* 14:7387–7400. <https://doi.org/10.1007/s13399-023-03775-z>
32. Asefy Z, Ceferov SHZ (2021) Nanoparticles approaches in neurodegenerative diseases diagnosis and treatment. *Neurol Sci* 42:2653–2660. <https://doi.org/10.1007/s10072-021-05234-x>
33. Mohammadi L, Pal K, Bilal M, Rahdar A, Fytianos G, Kyzas GZ (2021) Green nanoparticles to treat patients with malaria disease: An overview. *J Mol Struct* 1229:1–8. <https://doi.org/10.1016/j.molstruc.2020.129857>
34. Wolny-Koładka K, Malina D, Suder A, Pluta K, Wzorek Z (2022) Bio-based synthesis of silver nanoparticles from waste agricultural biomass and its antimicrobial activity. *Processes* 10(2):1–17. <https://doi.org/10.3390/pr10020389>
35. Hematizadeh A, Ebrahimzadeh MA, Sarvi S, Sadeghi M, Daryani A, Gholami S, Nayeri T, Hosseini SA (2023) *In vitro* and *in vivo* anti-parasitic activity of *Sambucus ebulus* and *Feijoa sellowiana* extracts silver nanoparticles on *Toxoplasma gondii* Tachyzoites. *Acta Parasitol* 68:557–565. <https://doi.org/10.1007/s11686-023-00689-8>
36. Arsène MMJ, Viktorovna PI, Alla M, Mariya M, Nikolaevitch SA, Davares AKL, Yurievna ME, Rehailia M, Gabin AA, Alekseevna KA, Vyacheslavovna YN, Vladimirovna ZA, Svetlana O, Milana D (2023) Antifungal activity of silver nanoparticles prepared using *Aloe vera* extract against *Candida albicans*. *Vet World* 16(1):18–26. <https://doi.org/10.14202/vetworld.2023.18-26>
37. Salvioni L, Galbiati E, Collico V, Alessio G, Avvakumova S, Corsi F, Tortora P, Prosperi D, Colombo M (2017) Negatively charged silver nanoparticles with potent antibacterial activity and reduced toxicity for pharmaceutical preparations. *Int J Nanomedicine* 12:2517–2530. <https://doi.org/10.2147/IJN.S127799>
38. Ali R, Islamuddin M, Tabrez S, Alsaweed M, Alaidarous MA, Alshehri BM, Banawas S, Dukhyil AAB, Rub A (2021) *Embilica officinalis* L. inhibits the growth and proliferation of *Leishmania donovani* through the induction of ultrastructural changes, mitochondrial dysfunction, oxidative stress and apoptosis-like cell death. *Biomed Pharmacother* 143:1–10. <https://doi.org/10.1016/j.biopha.2021.112156>
39. Keshav P, Goyal DK, Kaur S (2021) GC-MS screening and antiparasitic action of *Putranjiva roxburghii* leaves against sensitive and resistant strains of *Leishmania donovani*. *J Parasit Dis* 45:1002–1013. <https://doi.org/10.1007/s12639-021-01388-9>
40. Pramanik PK, Paik D, Pramanik A, Chakraborti T (2019) White jute (*Corchorus capsularis* L.) leaf extract has potent leishmanicidal activity against *Leishmania donovani*. *Parasitol Int* 71:41–45. <https://doi.org/10.1016/j.parint.2019.03.012>
41. Zahir AA, Chauhan IS, Bagavan A, Kamaraj C, hi Elango, Shankar J, Arjaria N, Roopan M, Rahuman AA, Singh N, (2014) Synthesis of nanoparticles using *Euphorbia prostrata* extract reveals a shift from apoptosis to G0/G1 arrest in *Leishmania donovani*. *J Nanomedicine & Nanotechnol* 5:1–12. <https://doi.org/10.4172/2157-7439.1000213>
42. Kumar V, Gundampati RK, Singh DK, Jagannadham MV, Sundar S, Hasan SH (2016) Photo-induced rapid biosynthesis of silver nanoparticles using aqueous extract of *Xanthium strumarium* and its antibacterial and antileishmanial activity. *J Ind Eng Chem* 37:224–236. <https://doi.org/10.1016/j.jiec.2016.03.032>
43. Baranwal A, Chiranjivi AK, Kumar A, Dubey VK, Chandra P (2018) Design of commercially comparable nanotherapeutic agent against human disease-causing parasite, *Leishmania*. *Sci Rep* 8:1–10. <https://doi.org/10.1038/s41598-018-27170-1>
44. Prasanna P, Kumar P, Mandal S, Payal T, Kumar S, Hossain SU, Das P, Ravichandiran V, Mandal D (2021) 7,8-dihydroxyflavone-functionalized gold nanoparticles target the arginase enzyme of *Leishmania donovani*. *Nanomedicine (Lond)* 16:1887–1903. <https://doi.org/10.2217/nmm-2021-0161>
45. Chakraborty S, Bhar K, Saha S, Chakraborti R, Pal A, Siddhanta A (2014) Novel arsenic nanoparticles are more effective and less toxic than As (III) to inhibit extracellular and intracellular proliferation of *Leishmania donovani*. *J Parasitol Res* 2014:1–10. <https://doi.org/10.1155/2014/187640>
46. Mishra S, Kumavat S (2022) Green Synthesis, characterization and antimicrobial activity of silver nanoparticles using *Uraria picta* leaves extract. *Micro Nanosyst* 14:212–225. <https://doi.org/10.2174/1876402913666210902161849>
47. Pathak P, Kumari A, Chandler BD, Zettler LW (2023) *In vitro* propagation and phytochemical analysis of *Vanda cristata* Wall. ex Lindl.: An endangered medicinal orchid of biopharmaceutical importance. *S Afr J Bot* 153:109–123
48. Olivier MT, Muganza FM, Shai LJ, Gololo SS, Nmutavhanani LD (2017) Phytochemical screening, antioxidant and antibacterial activities of ethanol extracts of *Asparagus suaveolens* aerial parts. *S Afr J Bot* 108:41–46
49. Jahan S, Tamta S, Shankhdhar SC, Shankhdhar D (2023) Salicylic acid potential to reversing drought induced oxidative stress in *Bacopa monnieri* (L.) through enhancement of bioactive compound (Bacoside-A) and antioxidants including physio-biochemical attributes. *S Afr J Bot* 161:617–626

50. Dilbar S, Sher H, Ali A, Ullah Z, Ali I (2023) Biological synthesis of Ag-nanoparticles using *Stachys parviflora* and its inhibitory potential against *Xanthomonas campestris*. *S Afr J Bot* 157:409–422
51. Aleixandre-Tudo JL, Toit Wd (2018) The role of UV-Visible spectroscopy for phenolic compounds quantification in wine-making. In: Solis-Oviedo RL and Pech-Canul AdIC (ed) Frontiers and new trends in the science of fermented food and beverages. IntechOpen. <https://doi.org/10.5772/intechopen.79550>
52. Banerjee S, Kar P, Islam R, Naidoo D, Roy A, Sarkar I, Sen G, Saha T, Yasmin H, Sen A (2022) Synthesis of silver nanoparticles from secondary metabolites of star gooseberry fruit (*Phyllanthus acidus*) and their nephroprotective efficiency. *S Afr J Bot* 151:385–395
53. Moshahary S, Mishra P (2021) Synthesis of silver nanoparticles (AgNPs) using culinary banana peel extract for the detection of melamine in milk. *J Food Sci Technol* 58:797–804. <https://doi.org/10.1007/s13197-020-04791-x>
54. Jeung DG, Lee M, Paek SM, Oh JM (2021) Controlled growth of silver oxide nanoparticles on the surface of citrate anion intercalated layered double hydroxide. *Nanomater* 11:1–15. <https://doi.org/10.3390/nano11020455>
55. Kumar V, Singh DK, Mohan S, Gundampati RK, Hasan SH (2017) Photoinduced green synthesis of silver nanoparticles using aqueous extract of *Physalis angulata* and its antibacterial and antioxidant activity. *J Environ Chem Eng* 5:744–756
56. Barros CHNd, Cruz GCF, Mayrink W, Tasic L (2018) Bio-based synthesis of silver nanoparticles from orange waste: effects of distinct biomolecule coatings on size, morphology, and antimicrobial activity. *Nanotechnol Sci Appl* 11:1–14. <https://doi.org/10.2147/NSA.S156115>
57. Ahmad A, Syed F, Shah A, Khan Z, Tahir K, Khan AU, Yuan Q (2015) Silver and gold nanoparticles from *Sargentodoxa cuneata*: synthesis, characterization and antileishmanial activities. *RSC Adv* 5:73793–73806. <https://doi.org/10.1039/C5RA13206A>
58. Ghosh S, Jagtap S, More P, Shete UJ, Maheshwari NO, Rao SJ, Kitture R, Kale S, Bellare J, Patil S, Pal JK (2015) Chopade BA (2015) *Dioscorea bulbifera* mediated synthesis of novel Au_{core}Ag_{shell} nanoparticles with potent antibiofilm and antileishmanial activity. *J Nanomater* 562938:1–12. <https://doi.org/10.1155/2015/562938>
59. Ahmad A, Syed F, Imran M, Khan AU, Tahir K, Khan ZUH, Yuan Q (2016) Phytosynthesis and antileishmanial activity of gold nanoparticles by *Maytenus Royleanus*. *J Food Biochem* 40:420–427. <https://doi.org/10.1111/jfbc.12232>
60. Zhou X, Meng Z, She J, Zhang Y, Yi X, Zhou H, Zhong J, Dong Z, Han X, Chen M, Fan Q, Yang K, Wang C (2020) Near-Infrared light-responsive nitric oxide delivery platform for enhanced radioimmunotherapy. *Nano-Micro Lett* 12. <https://doi.org/10.1007/s40820-020-00431-3>
61. Balashanmugam P, Balakumaran MD, Murugan R, Dhanapal K, Kalaichelvan PT (2016) Phytochemical synthesis of silver nanoparticles, optimization and evaluation of *in vitro* antifungal activity against human and plant pathogens. *Microbiol Res* 192:52–64. <https://doi.org/10.1016/j.micres.2016.06.004>
62. Rahman G, Fazal H, Ullah A, Ahmad S, Nadeem T, Ahmad M, Ahmad I, Mishra N, Ashique S, Zengin G, Farid A (2024) Empowering silver and copper nanoparticles through aqueous fruit extract of *Solanum xanthocarpum* for sustainable advancements. *Biomass Convers Biorefin*. <https://doi.org/10.1007/s13399-024-05270-5>
63. Padi PM, Adetunji TL, Unuofin JO, Mchunu CN, Ntuli NR, Siebert F (2022) Phytochemical, antioxidant, and functional group analyses of South African *Evolvulus alsinoides* (L.) L. *S Afr J Bot* 149:170–177. <https://doi.org/10.1016/j.sajb.2022.06.005>
64. Mohammed MHH, Hamed ANE, Elhabal SF, Mokhtar FA, Abdelmohsen UR, Fouad MA, Kamel MS (2023) Metabolic profiling and cytotoxic activities of ethanol extract of *Dypsis leptocheilos* aerial parts and its green synthesized silver nanoparticles supported by network pharmacology analysis. *S Afr J Bot* 161:648–665. <https://doi.org/10.1016/j.sajb.2023.08.026>
65. Restrepo CV, Villa CC (2021) Synthesis of silver nanoparticles, influence of capping agents, and dependence on size and shape: A review. *Environ Nanotechnology Monit Manag* 15:1–11. <https://doi.org/10.1016/j.enmm.2021.100428>
66. Foroozandeh P, Aziz AA (2018) Insight into cellular uptake and intracellular trafficking of nanoparticles. *Nanoscale Res Lett* 13(339):1–12. <https://doi.org/10.1186/s11671-018-2728-6>
67. Al-Sheddi ES, Alsohaibani N, Rshoud N, Al-Oqail MM, Al-Massarani SM, Farshori NF, Malik T, Al-Khedhairi AA, Siddiqui MA (2023) Anticancer efficacy of green synthesized silver nanoparticles from *Artemisia monosperma* against human breast cancer cells. *S Afr J Bot* 160:123–131. <https://doi.org/10.1016/j.sajb.2023.07.001>
68. Pizzagalli L, Brochard S, Godet J, Durinck J (2024) The structural stability of tungsten nanoparticles. *Beta Arxiv*. arXiv:2404.04161v1 [cond-mat.mtrl-sci]
69. Khan I, Saeed K, Khan I (2019) Nanoparticles: Properties, applications and toxicities. *Arab J Chem* 12(7):908–931. <https://doi.org/10.1016/j.arabjc.2017.05.011>
70. Ameen F, Alown F, Al-Owaidi MF, Sivapriya T, Ramirez-Coronel AA, Khat M, Akhavan-Sigari R (2023) African plant-mediated biosynthesis of silver nanoparticles and evaluation of their toxicity, and antimicrobial activities. *S Afr J Bot* 156:213–222. <https://doi.org/10.1016/j.sajb.2023.03.010>
71. Chen LQ, Fang L, Ling J, Ding CZ, Kang B, Huang CZ (2015) Nanotoxicity of silver nanoparticles to red blood cells: size dependent adsorption, uptake, and hemolytic activity. *Chem Res Toxicol* 28:501–509. <https://doi.org/10.1021/tx500479m>
72. Stoehr LC, Gonzalez E, Stampfl A, Casals E, Duschl A, Puentes V, Oostingh GJ (2011) Shape matters: effects of silver nanospheres and wires on human alveolar epithelial cells. *Part Fibre Toxicol* 8:1–15. <https://doi.org/10.1186/1743-8977-8-36>
73. Jaffri SB, Ahmad KS (2020) Biomimetic detoxifier *Prunus cerasifera* Ehrh. Silver nanoparticles: innate green bullets for morbidic pathogens and persistent pollutants. *Environ Sci Pollut Res* 27:9669–9685
74. Singh AK, Tiwari R, Kumar V, Singh P, Khadim SKR, Tiwari A, Srivastava V, Hasan SH, Asthana RK (2017) Photo-induced biosynthesis of silver nanoparticles from aqueous extract of *Dunaliella salina* and their anticancer potential. *J Photochem Photobiol B* 166:202–211. <https://doi.org/10.1016/j.jphotobiol.2016.11.020>
75. Atrooz O, Al-Nadaf A, Uysal H, Kutlu HM, Sezer CV (2023) Biosynthesis of silver nanoparticles using *Coriandrum sativum* L. extract and evaluation of their antibacterial, anti-inflammatory and antinociceptive activities. *S Afr J Bot* 157:219–227. <https://doi.org/10.1016/j.sajb.2023.04.001>
76. Raja S, Ramesh V, Thivaharan V (2017) Green biosynthesis of silver nanoparticles using *Calliandra haematocephala* leaf extract, their antibacterial activity and hydrogen peroxide sensing capability. *Arab J Chem* 10:253–261. <https://doi.org/10.1016/j.arabjc.2015.06.023>
77. Badawy AME, Silva R, Morris B, Scheckel KG, Suidan MT, Tolaymat TM (2011) Surface charge-dependent toxicity of silver nanoparticles. *Environ Sci Technol* 45:283–287. <https://doi.org/10.1021/es1034188>
78. Chen Y, Li J, Yue G, Luo X (2017) Novel Ag@Nitrogen-doped porous carbon composite with high electrochemical performance as anode materials for lithium-ion batteries. *Nanomicro Lett* 9:1–11. <https://doi.org/10.1007/s40820-017-0131-y>

79. Botcha S, Prattipati SD (2023) Antioxidant, antimetastatic and apoptotic potential of silver nanoparticles synthesized by leaf and callus extracts of *Hyptis suaveolens* L. *S Afr J Bot* 160:36–45. <https://doi.org/10.1016/j.sajb.2023.06.055>
80. Corrêa AdS, Contreras LA, Keijok WJ, Barcelos DHF, Pereira ACH, Kitagawa RR, Scherer R, Gomes DCdO, Silva ARd, Endringer DC, Oliveira JPd, Guimaraes MCC (2018) *Viola oleifera*-capped gold nanoparticles showing radical-scavenging activity and low cytotoxicity. *Mater Sci Eng C* 91:853–858. <https://doi.org/10.1016/j.msec.2018.06.027>
81. Ullah I, Cosar G, Abamor ES, Bagirova M, Shinwari ZK, Allah-verdiyev AM (2018) Comparative study on the antileishmanial activities of chemically and biologically synthesized silver nanoparticles (AgNPs). *3 Biotech* 8:1–8. <https://doi.org/10.1007/s13205-018-1121-6>
82. Chakraborty S, Bhar K, Saha S, Chakrabarti R, Pal A (2014) Sidhanta, A (2014) Novel Arsenic nanoparticles are more effective and less toxic than As (III) to inhibit extracellular and intracellular proliferation of *Leishmania donovani*. *J Parasitol Res* 187640:1–10. <https://doi.org/10.1155/2014/187640>
83. Mukherjee S, Chowdhury D, Kotcherlakota R, Patra S, Vinothkumar B, Bhadra MP, Sreedhar B, Patra CR (2014) Potential theranostics application of bio-synthesized silver nanoparticles (4-in-1 system). *Theranostics* 4:316–335. <https://doi.org/10.7150/thno.7819>
84. Mariño G, Kroemer G (2013) Mechanisms of apoptotic phosphatidylserine exposure. *Cell Res* 23:1247–1248. <https://doi.org/10.1038/cr.2013.115>
85. Ebrahimzadeh MA, Hashemi Z, Mohammadyan M, Fakhar M, Mortazavi-Derazkola S (2021) *In vitro* cytotoxicity against human cancer cell lines (MCF-7 and AGS), antileishmanial and antibacterial activities of green synthesized silver nanoparticles using *Scrophularia striata* extract. *Surfaces and Interfaces*. <https://doi.org/10.1016/j.surfin.2021.100963>
86. Mohammadi M, Zaki L, KarimiPourSaryazdi A, Tavakoli P, Tava-jjohi A, Poursalehi R, Delavari H, Ghaffarifar F (2021) Efficacy of green synthesized silver nanoparticles via ginger rhizome extract against *Leishmania major* *in vitro*. *PLoS ONE* 16:1–12. <https://doi.org/10.1371/journal.pone.0255571>
87. Moradin N, Descoteaux A (2012) *Leishmania* promastigotes: building a safe niche within macrophages. *Front Cell Infect Microbiol* 2:1–7. <https://doi.org/10.3389/fcimb.2012.00121>
88. Silva-Almeida M, Pereira BAS, Ribeiro-Guimarães ML, Alves CR (2012) Proteinases as virulence factors in *Leishmania* spp. infection in mammals. *Parasit Vectors* 5(160):1–10. <https://doi.org/10.1186/1756-3305-5-160>
89. Anamika Singh R, Manar KK, Yadav CL, Kumar A, Singh RK, Drew MGB, Singh N (2019) Impact of substituents on the crystal structures and anti-leishmanial activity of new homoleptic Bi(iii) dithiocarbamates. *New J Chem* 43:16921–16931. <https://doi.org/10.1039/C9NJ04477A>

Publisher's Note Springer Nature remains neutral with regard to jurisdictional claims in published maps and institutional affiliations.

Springer Nature or its licensor (e.g. a society or other partner) holds exclusive rights to this article under a publishing agreement with the author(s) or other rightsholder(s); author self-archiving of the accepted manuscript version of this article is solely governed by the terms of such publishing agreement and applicable law.